Food Chemistry: X 24 (2024) 101895

Contents lists available at ScienceDirect

Food Chemistry: X

journal homepage: www.sciencedirect.com/journal/food-chemistry-x

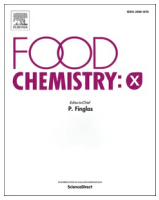

Optimization of ultrasonication assisted extraction of *Aegle marmelos* fruit shell nano polysaccharide and evaluation of photocatalytic dye reduction and edible coating for fresh-cut fruits

Madhu Sharma [a], Aarti Bains [b], Gulden Goksen [c], Nemat Ali [d], Mohammad Rashid Khan [d], Gulsah Karabulut [e,*], Prince Chawla [a,*]

[a] Department of Food Technology and Nutrition, Lovely Professional University, Phagwara, Punjab 144411, India
[b] Department of Microbiology, Lovely Professional University, Phagwara, Punjab 144411, India
[c] Department of Food Technology, Vocational School of Technical Sciences at Mersin Tarsus Organized Industrial Zone, Tarsus University, 33100 Mersin, Turkey
[d] Department of Pharmacology and Toxicology, King Saud University, P.O. Box 2457, Riyadh 11451, Saudi Arabia
[e] Department of Food Engineering, Faculty of Engineering, Sakarya University, 54050, Sakarya,Turkey

ARTICLE INFO

Keywords:
Ultrasonication
Aegle marmelos shell
Polysaccharide
Photocatalytic dye reduction
Edible coating

ABSTRACT

Aegle marmelos (AM) fruit shell, considered waste, is an excellent source of bioactive compounds, including polysaccharides. Therefore, this study focuses on the extraction of AM polysaccharides using an ultrasonication-assisted approach. Different parameters, including ultrasonic power (200–600 W), time (5–15 min), and solid-to-solvent ratio (10–20 mg/mL), were employed, and significantly ($p < 0.05$) higher yield (16.93 %) was achieved at 400 W for 10 min. Monosaccharides composition revealed galactose (30.56 ± 0.76 %), galacturonic acid (24.72 ± 0.12 %), arabinose (17.26 ± 0.35 %), xylose (11.48 ± 0.21 %), glucose (10.52 ± 0.26 %), and rhamnose (5.39 ± 0.67 %), which were then confirmed by ^{13}C spectrum. AM polysaccharides revealed nanoscale size with excellent structural crystallinity and thermal stability. Edible coatings of varying concentrations (0.5–2 %) were formulated and optimized 1 % coating, demonstrating efficacy in mitigating weight loss, microbial proliferation, and browning in cut apples. As well, AM polysaccharides prominently degraded 82.79 ± 0.39 % of methyl green. Overall, bael shells as a valuable source of polysaccharides, offering the potential for both photocatalytic dye degradation and food preservation.

1. Introduction

Aegle marmelos is a member of the Rutaceae family, commonly known as Bael and potentially used for the formulation of Indian traditional medicines. It originated in northern India but is extensively found in different parts of the world including Indo-China, Thailand, Bangladesh, Burma, and Ceylon (Mahato & Kumar, 2022). Morphologically, the plant possesses globular fruits, short flowers, and 3 cm long trifoliate leaves. While the pulp of this fruit is widely recognized for its nutritional and medicinal properties including digestive aid and immune system support, its shell often remains an underutilized waste product (Sharma et al., 2022). The shell of the *Aegle marmelos* fruit, sometimes seen as waste, holds significant possibilities for value addition owing to its abundant biological components, including polysaccharides.

Polysaccharides are complex carbohydrates that have attracted considerable interest recently because of their versatile properties and potential applications across various industries (Yang et al., 2020). These biopolymers consist of different monosaccharide units (glucose, fructose, or galactose, or more complex sugars like glucuronic acid or N-acetylglucosamine) linked together through glycosidic bonds. The specific arrangement and types of monosaccharide units within the polymer chain determine the unique properties and functionalities of each polysaccharide (Colusse et al., 2022). Their chemical structures and functionalities vary widely, offering a broad spectrum of applications. These biopolymers are biocompatible, and biodegradable, making them environmentally friendly alternatives to synthetic materials (Mtibe et al., 2021). Moreover, polysaccharides exhibit remarkable functional properties including gelation, thickening, and stabilization, which make them valuable ingredients in food and pharmaceutical sectors.

* Corresponding authors.
E-mail addresses: gkarabulut@sakarya.edu.tr (G. Karabulut), princefoodtech@gmail.com (P. Chawla).

https://doi.org/10.1016/j.fochx.2024.101895
Received 31 August 2024; Received in revised form 4 October 2024; Accepted 10 October 2024
Available online 15 October 2024

Traditionally, the extraction of polysaccharides from natural sources has primarily depended on conventional methods, including chemical precipitation and hot water extraction (C. Wang et al., 2023). However, these methods often exhibit several drawbacks, including low extraction efficiency, prolonged processing times, and the utilization of potentially hazardous chemicals, which can compromise the quality of the extracted polysaccharides (Shengyi Zhou et al., 2020). In response to these challenges, researchers have increasingly turned to novel extraction techniques such as supercritical fluid extraction, microwave-assisted extraction, pulsed electric field, and ultrasonication to overcome these limitations and enhance the overall extraction process (Jönsson et al., 2020). Among these innovative approaches, ultrasonication has emerged as a promising method for polysaccharide extraction.

Ultrasonication involves the utilization of high-frequency vibrations (sound waves) to disrupt cell walls and facilitate the release of bioactive compounds, including polysaccharides, from plant materials (Gouda et al., 2021). The ultrasonic waves cause the formation and collapse of tiny bubbles which generate intense mechanical forces, including microstreaming and shockwaves rupture cell structures, and increase the diffusion of polysaccharides into the surrounding solvent. The key advantage of ultrasonication is its ability to significantly enhance extraction yields compared to traditional methods (Khadhraoui et al., 2021). The mechanical forces generated by ultrasonic waves enable more efficient disruption of cell walls, allowing for a greater release of polysaccharides into the solvent (Biswas & Rashid, 2022). This increased extraction efficiency is particularly beneficial for extracting polysaccharides from tough or fibrous plant matrices that are resistant to conventional extraction techniques. Moreover, ultrasonication offers the advantage of reduced processing times. The rapid energy transfer associated with ultrasound waves accelerates mass transfer kinetics, leading to shorter extraction durations.

The environmental impact of artificial dyes utilized across diverse sectors such as textiles, cosmetics, and food processing, has become a growing concern (Slama et al., 2021). These dyes are often released into water bodies as effluents, leading to water pollution and ecological damage. Furthermore, the rapid decay of cut fruits, such as apples, during storage and transportation contributes to food wastage and economic losses (Onwude et al., 2020). Addressing these challenges requires innovative solutions that can simultaneously extend the shelf life of perishable goods and mitigate environmental harm.

Polysaccharides derived from *Aegle marmelos* fruit shells offer multifunctional properties that can address both environmental and food preservation challenges (Gaikwad, Sutar, & Patil, 2024). These polysaccharides have exhibited remarkable efficacy in photocatalytic dye removal, aiding in the remediation of dye-polluted water bodies. The ability of polysaccharides to serve as electron donors or acceptors in redox reactions is responsible for their photocatalytic activity, leading to the degradation of dye molecules under light irradiation (Sarkar et al., 2020). Additionally, the utilization of polysaccharide-based edible coatings on cut fruits, such apples, has demonstrated their ability to prolong shelf life through providing a protective barrier against microbial contamination and moisture loss (Aayush et al., 2022). Thus, this research focused on the utilization of *Aegle marmelos* fruit shell polysaccharides, which is a sustainable and innovative approach to value addition and waste reduction in the agricultural and food processing industries. New extraction techniques, such as ultrasonication, can maximize the yield and bioactivity of polysaccharides while reducing environmental impact. Furthermore, the multifunctional properties of polysaccharides offer promising solutions to address both environmental pollution from synthetic dyes and food wastage due to rapid fruit decay. Overall, the potential of polysaccharides from *Aegle marmelos* fruit shells can be fully recognized, contributing to the advancement of circular economy principles and sustainable development.

2. Materials and methods

2.1. Materials

Aegle marmelos fruit shell was collected from the wild area of Jalandhar, Punjab, India. For the coating application, apples were purchased from the supermarket (Phagwara, Punjab, India), and stored at 4–7 °C until processing. Chemicals used in this study including sodium carbonate, sodium hydroxide (NaOH), potato dextrose agar, potassium bromide (KBr), nutrient agar, trifluoroacetic acid (TFA), 1-phenyl-3-methyl-5-pyrazolone (PMP), phenolphthalein indicator, and Folin–Ciocalteu reagent were acquired from the Loba Chem Pvt. Ltd. (Mumbai, India).

2.2. Proximate analysis

Carbohydrates, fat, moisture, ash, protein, and crude fiber were assessed by the methodology conducted by Abbas et al. (2021). Moisture content was evaluated by using the oven drying technique at a temperature of 105 °C. Ash content was determined using a muffle furnace heated to approximately 550 °C for 6 h. The protein content was determined using the Kjeldahl method. The analysis of crude fiber content involved acid (H_2SO_4) and alkali (NaOH) digestion methods. Crude fat content was analyzed through extraction using a Soxhlet apparatus with hexane for 5–6 h. Carbohydrate content was calculated using the difference method and all the compositions are expressed as percentages (%).

2.3. Extraction of polysaccharide

Aegle marmelos fruit shell polysaccharide was extracted utilizing ultrasonication-assisted extraction by following the methodology described by Hu et al. (2022) with certain modifications in frequency and solvent ratio. Extraction was conducted by probe ultrasonicator (EchoWave 5000, SonicPulse Ultrasonics, California, USA) using different power, time, and solid-to-solvent ratio combinations (200–600 W, 5–15 min, and 10–20 mg/mL solid-to-solvent ratio). The obtained extract was filtered to remove the insoluble fractions and then centrifuged at 8000 rpm for 20 min. Following centrifugation, the supernatant was collected and dried in a Spraytech Lab Scale Spray Dryer (Spraytech Systems Pvt. Ltd., Mumbai, India). The spray drying conditions were determined based on our previously optimized study of spray drying of polysaccharides (M. Sharma et al., 2023). The process involved an inlet temperature of 160 °C, an outlet temperature of 70 °C, an atomizer speed set at 2400 rpm, and a feed flow rate of 7 mL/min. The yield of extracted powder was calculated on a dry basis as per the following Eq. (1).

$$\text{Yield } (\%) = \left[\left(\frac{\textit{Weight of dried powder } (g)}{\textit{Total weight of shell powder } (g)} \right) \times 100 \right] \quad (1)$$

2.3.1. Experimental design

The optimization of ultrasonication conditions for extracting *Aegle marmelos* fruit shell polysaccharides (AMFSP) was performed using Box-Behnken design (Response Surface Methodology), employing three independent variables. A total of 15 experimental runs were conducted, varying ultrasonication power (200–600 W), time (5–15 min), and solid to solvent ratio (10–20 mg/mL). The model significance was assessed through ANOVA (analysis of variance) and lack of fit was conducted with a confidence level of 95 %. A second-degree polynomial regression model investigated the interplay between multiple independent variables (solid-to-solvent ratio, ultrasonication power, and time) and the dependent variables (extraction and polysaccharide yield), as expressed in Eq. (2).

$$Y_k = \beta_\circ + \beta_1 A + \beta_2 B + \beta_3 C + \beta_4 A^2 + \beta_5 B^2 + \beta_6 C^2 + \beta_7\ AB + \beta_8\ BC + \beta_9 AC \quad (2)$$

In the equation, Yk represents the response variable, where Y1 signifies the extraction yield (%) and Y2 indicates the polysaccharide yield (%). The variables A, B, and C correspond to the independent variables representing ultrasonication power, time, and solid-to-solvent ratio, respectively. The value of the response predicted at the midpoint of the experimental design is represented by β∘. The coefficients β1, β2, and β3 stand for the coefficients of the linear regression, while β4, β5, and β6 denote the coefficients of the quadratic regression, and β7, β8, and β9 indicate the coefficients of the cross-product regression. The coefficient of determination, R^2, is employed for the assessment of the efficiency of the model.

2.3.2. Total carbohydrate content

The total carbohydrate content of the ultrasonicated extracted *Aegle marmelos* fruit shell powder was assessed using the phenol sulfuric acid method in which glucose was used as standard solution from 0 to 100 μg/mL concentration (Medlej et al., 2020). Briefly, an aliquot of 100 μL standard solution was mixed with 100 μL of 5 % (*v*/v) phenol and 500 μL of concentrated sulfuric acid followed by incubating the sample for 15 min at 80 °C (water bath) then cooled to room ambient temperature. Absorbance was measured at 490 nm using a spectrophotometer and plotted a calibration curve against glucose concentrations. The carbohydrate content of the sample was calculated based on its absorbance and the calibration curve.

2.4. Characterization of AMFSP

2.4.1. Monosaccharide composition

The monosaccharide composition of AMFSP was analyzed following the method described by Bazezew et al. (2022) using high-performance liquid chromatography (HPLC). Initially, 50 mg of AMFSP underwent hydrolysis with 5 mL of 2 M TFA solution in a sealed glass tube at 100 °C for 2 h. The removal of excess acids was achieved by multiple washes with 80 % ethanol to ensure complete elimination. Subsequently, labeling was initiated by adding 2 mL of 10 M NaOH and 1 mL of 0.10 M PMP solution to the dried hydrolysis product, followed by incubation at 80 °C for 2 h. Neutralization was performed by adding 0.1 mL of 0.1 M HCl solution, followed by three extractions with chloroform. The resulting aqueous phase was filtered through a 0.50 μm nylon membrane for sugar analysis. The prepared solution was then injected into an RPC18 column using a mobile phase comprising acetonitrile and 0.2 M phosphate buffer (20:80, pH = 6.7) at a flow rate of 1.0 mL/min, with an injection volume of 25 μL. Standard monosaccharides were analyzed using the same method for comparison, and the sugar content of AMFSP was determined by comparing the retention times of standard sugars.

2.4.2. Fourier transform infrared spectroscopy (FTIR)

The procedure outlined by Olawuyi et al. (2020) was utilized to determine the functional groups of AMFSP using a Cary 630 FTIR spectrophotometer (Agilent Technologies, Santa Clara, California, USA). The powdered AMFSP sample was combined with KBr in a 1:100 ratio and pressed to form pellets. Following this, the FTIR spectrometer is calibrated with a background spectrum run to correct for atmospheric absorption. The prepared KBr pellets were then placed on the sample holder of the spectrometer and scanned over a range of 4000–400 cm^{-1} with a resolution of 4 cm^{-1}. The spectra were generated by averaging 32 individual scans to ensure accuracy and reproducibility.

2.4.3. Nuclear magnetic resonance (NMR) analysis

The AMFSP underwent NMR analysis using a JEOL Avance III spectrometer operating at 500 MHz. Both 1H and 2D ^{1}H-^{1}H COSY NMR spectra were recorded, following the procedure outlined by Wang et al. (2022). The dried powdered sample (40 mg) was dissolved in 1 mL D_2O (deuterium oxide) for repeated freeze-drying. The experiments were carried out at 25 °C, with a pulse delay of 1.0 s, and D_2O was used as the solvent. The NMR spectra were calibrated using the residual HOD signal at 4.79 ppm.

2.4.4. Differential scanning calorimetry (DSC)

The thermal properties of AMFSP powder were assessed using the DSC-60 Plus instrument (Shimadzu, Kyoto, Japan) ((Sharma et al., 2023). The instrument was calibrated with standard materials such as indium and zinc. Briefly, 5 mg of the polysaccharide powder was weighed and sealed within an aluminum pan, while a reference pan was left empty. Before the DSC run, both the sample and reference pans were uniformly heated under an inert nitrogen atmosphere (99.999 %) to mitigate oxidation effects. The DSC was then programmed to gradually increase the temperature from 10 °C to 450 °C, at a controlled rate of 10 °C/min. The data was recorded using temperature sensors based on thermocouples, and graphs were generated.

2.4.5. Thermogravimetric analysis (TGA)

The mass loss and thermal degradation of the AMFSP were determined using the Mettler Toledo TGA instrument (Schwerzenbach, Switzerland) (X. Liu et al., 2020). Following calibration, 15 mg of AMFSP powder sample was put in the TGA platinum pan. The analysis proceeds by heating the sample from 10 °C to 950 °C at a consistent heating rate of 10 °C/min under a 50 mL/min N_2 (99.999 %) atmosphere to prevent oxidative degradation of the polysaccharides. The instrument automatically records the weight change in the sample relative to temperature.

2.4.6. Particle size and surface charge

The powdered AMFSP was evaluated for its particle size and zeta potential using Brookhaven Instruments (Holtsville, NY, USA) (Shengnan Wang et al., 2020). Briefly, 100 mg of powdered AMFSP was dispersed in 20 mL of deionized water within 50 mL glass vials, followed by ultrasonication using a bath sonicator (Malvern-Aimil Instruments, India). Measurements were performed in triplicates at 25 °C using the clean cuvettes for each sample.

2.4.7. Scanning Electron Microscopy (SEM)

The morphological characteristics of AMFSP were analyzed using a field emission scanning electron microscope (JEOL JSM-7610F Plus) as described by Su and Li (2020) A 5 mg sample of powdered sample was affixed to an aluminum pan holder using conductive tape, and subsequently coated with gold-palladium at 20 mA for 2 min. Micrographs were obtained at magnifications of 250× with working distances of 8.0 mm respectively, and an accelerating voltage of 20 kV.

2.4.8. X-ray diffraction (XRD)

The AMFSP sample was evaluated for XRD analysis using a Bruker D8 Advance instrument (Bruker AXS, Madison, WI, USA), according to the previous methodology (Savi et al., 2020). In brief, a 10 mg sample was placed in a sample holder and the measurements were conducted at 40 kV, with Cu-Kα radiation, scanning from 10° to 50° at a 2θ angle.

2.5. Photocatalytic dye reduction

The dye reduction efficacy of polysaccharides against methyl green was carried out following the methodology given by Guleria et al. (2024) under UV light irradiation using a 30 W UV lamp (Indetouch Exporters Enterprise Tambaram, Tamil Nadu, India). Initially, a 25 mL aqueous suspension containing 100 μL of AMFSP solution and methyl green dye was prepared. Subsequently, the mixture was stirred for 30

min in the dark to achieve equilibrium between the adsorption and desorption processes followed by exposure to UV light. At regular 10-min intervals, solution samples of 2 mL were extracted and then centrifuged at 10,000 rpm for 8 min. The alteration in dye absorbance at its maximum wavelength (200–800 nm) was monitored using a spectrophotometer. The degradation (%) of methyl green dye was calculated by following Eq. (3)

$$\textit{Dye degradation efficiency}\ (\%) = [C_0 - C_t \times 100] \quad (3)$$

where C_o is the initial dye concentration while C_t indicates the amount of dye left at a certain time. Generally, the degradation of organic dyes follows the first-order kinetics, aligning with the Langmuir-Hinshelwood mechanism as defined in Eq. (4):

$$\left[ln\left(\frac{C_0}{C_t}\right) = kt\right] \quad (4)$$

where k is constant, which represents the first-order rate (min^{-1}). The slope of ln (C_o/C_t) plotted against irradiation time (t) was determined using the calculation of k (min^{-1}).

2.5.1. Scavenging activity

The scavenging activity test was performed to identify the primary and secondary contributors among photoactive species which was determined by following the method of Ahmad et al. (2022). Benzoquinone (BQ), ethylenediaminetetraacetic acid (EDTA), butyl alcohol (TBA), and silver nitrate (Ag NO3) were all employed to scavenge superoxide free radicals, holes, hydroxyl radicals, and free electrons, respectively, in order to verify the photoactive species involved in the degradation of methyl green dye. In this photocatalytic experiment, different trapping species were dissolved or mixed in the methyl green solution. The next procedure was identical to the aforementioned methyl green degradation process.

2.6. Preparation of coating solution

The coating solution of AMFSP at different concentrations was prepared according to Chettri et al. (2023) with slightly modifications. Briefly, the different amount of polysaccharides (0.5, 1, 1.5, and 2 % *w/v*) was taken and dispersed in 100 mL of water followed by the addition of 1.5 mL of glycerol and 3 mL of glacial acetic acid. Individually, the resulting solution was subjected to homogenization by magnetic stirring for 35 min at 80 °C. Based on particle size analysis, the solution exhibiting the smallest nanoparticles was selected for subsequent coating applications.

Uniform-colored fresh apple fruits were selected and disinfected using a solution of 0.1 % sodium hypochlorite. Following this, they were rinsed with distilled water, peeled using a clean stainless-steel knife, deseeded, and cut into small equal slices. The coating was then applied to fresh-cut apple fruit by immersing it in the coating solution for 2 min, then dried for 60 min at ambient temperature. A control group (uncoated samples) was also included. Both coated and uncoated samples were stored in sealed 2 cm × 4 cm polyethylene trays to prevent moisture and aroma changes. During a 10-day storage period at 4–7 °C, the samples were monitored for both physicochemical and microbiological quality parameters, at intervals of 2 days.

2.6.1. Rheological behavior

The rheology of the coating solution was analyzed using a Mettler Toledo Rheometer (RSX, Schwerzenbach, Switzerland). Briefly, 1 mL of the coating solution is applied to the rheometer plate, carefully ensuring complete coverage and the absence of air bubbles. A standardized pre-shearing was performed on the coating solution (1%1%) before applying a shear rate of 1-100 s-1 for 3 minutes at 25 °C to ensure consistency between samples.

2.7. Physiochemical properties of fresh-cut fruits

2.7.1. Color

The color of fresh-cut apples was measured during storage (0, 2, 4, 6, 8, and 10 days) using a HunterLab UltraScan VIS colorimeter (Hunterlab, Virginia, USA) by methodology given by Kathiresan and Lasekan (2019). Three color parameters were assessed, L* (lightness), a* (red/green), and b* (yellow/blue), according to the CIELAB (International Commission on Illumination's Lab color space). This measurement provides the fresh-cut fruit color, including its brightness, hue, and saturation. The study utilized the mean values from the three replications executed for each experiment. The ΔE value can be calculated using the following Eq. (5), while Browning index can be calculated using Eq. (6)

$$\Delta E = \left[\sqrt{(\Delta L)^2 + (\Delta a)^2 + (\Delta b)^2}\right] \quad (5)$$

$$\text{Browning index} = \left[100 \times \left(\frac{x - 0.31}{0.172}\right)\right] \quad (6)$$

$$x = \left[\left(\frac{a^* + 1.75\,L^*}{5.645\,L^* + a^* - 3.012b^*}\right)\right] \quad (7)$$

2.7.2. Weight loss

The fresh-cut apples were weighed at regular intervals (0, 2, 4, 6, 8, and 10 days of storage) to monitor weight loss over time using Wensar analytical balance (MAB201/301, India) (Tosif et al., 2023).

2.7.3. pH and acidity

The method performed by Oliveira Filho et al. (2022) was utilized to evaluate the alteration in the pH and acidity of the fresh-cut apples. Before measuring, the pH meter (Ohaus Starter 300 Portable pH Meter ST300, Ohaus Corporation, New Jersey, USA) was calibrated using standard buffer solutions (4 and 7). Subsequently, 10 g of apple, was homogenized with 50 mL of deionized water, and the mixture was filtered to obtain a clear juice. The pH meter probe was then immersed in the apple juice, and the pH value is recorded in triplicates for each sample.

For titratable acidity determination, 10 mL of the previously filtered apple juice was placed into a conical flask and was titrated with NaOH solution (0.1 M) with phenolphthalein indicator, and acidity was quantified as % relative to malic acid.

2.7.4. Total phenolic content (TPC)

The procedure performed by Soeung et al. (2022) was utilized to assess the polyphenol content of apple extract by employing the Folin–Ciocalteau regeant with gallic acid as the standard (0–300 μg/mL). The Folin-Ciocalteau reagent was combined with 100 μL of apple extract, and ultrapure water was added to increase the volume to 8.5 mL and allowed to react for 5 min. After the initial reaction, 1.5 mL of sodium carbonate having 20 % concentration was added to the mixture, followed by further heating at 45 °C for 25 min. The absorbance of the mixture was determined at 765 nm utilizing ultrapure water as a reference.

2.7.5. Antioxidant analysis

The DPPH (2,2-diphenyl-1-picryl-hidrazil) assay was determined the antioxidant activity of the apple extracts according to Tosif et al. (2023). Measure the change in absorbance at 517 nm to determine the antioxidant capacity and the calculated as (%) inhibition of DPPH scavenging activity using Eq. (8).

$$\text{Antioxidant activity (\%)} = \left[\left(\frac{Absorbance\ of\ sample - Absorbance\ of\ control}{Absorbance\ of\ sample}\right) \times 100\right] \quad (8)$$

2.7.6. Microbial analysis

The effect of storage on the total plate count, yeast, and mold counts on 0, 3, 6, 9, and 12th day were analyzed by applying the methodology with minor modifications (Tabassum and Khan, 2020). The surface of each apple is sterilized using 70 % ethanol before swabbing the entire area with sterile cotton swabs moistened with peptone water. The swabs are then transferred to sterile tubes containing peptone water and vortexed for 1 min to release the microbes. These solutions were serially diluted and plated on nutrient agar for total plate count, which were incubated at 37 °C for 24–48 h, and on potato dextrose agar for yeast and mold, with incubation at 25 °C for 3–5 days. After incubation, the number of colonies on each plate was counted, and these counts were used to calculate the colony-forming units (CFU) per square centimeter the of fruit surface.

2.7.7. Sensory analysis

Twenty male and female semi-trained panelists, ages 25–45, evaluated the sensory assessment of coated and control fresh-cut apples on 0 or 10th day of analysis. Both the apple samples were presented in dishes marked with random, anonymous codes to reduce the potential for bias. The panelists evaluated attributes such as flavor, texture, appearance, and overall acceptability using a nine-point hedonic scale.

2.8. Statistical analysis

Data was subjected to statistical analysis using SPSS software (SPSS, Inc., Armonk, NY, USA) and presented as mean ± standard deviation from triplicate experiments. Analysis of variance (ANOVA) and post-hoc tests were conducted to assess the significance of differences ($p \leq 0.05$).

3. Result and discussion

3.1. Proximate analysis

The proximate composition analysis of bael fruit shell powder revealed its nutritional profile, as outlined in Table 1A. The moisture, fat, ash, crude fiber, protein, and carbohydrate contents were found at 11.83 ± 0.28 %, 3.13 ± 0.23 %, 1.66 ± 0.28 %, 22.84 ± 1.27 %, 7.53 ± 0.90 %, and 53.01 ± 0.32 %, respectively. With its low moisture content, bael fruit shell powder demonstrates good stability, while moderate levels of fat and protein contribute to its nutritional diversity. Notably, bael fruit shell powder emerges as a rich source of polysaccharides (53.01 %) and crude fiber (22.84 %), highlighting its potential in various food applications. The ash content of 1.66 % indicates the presence of essential minerals. These results are consistent with the finding of Surolia et al. (2022) for the proximate composition of bael fruit shells. Overall, these findings underscore bael fruit shell powder significance as a valuable nutritional resource.

Table 1A
Proximate composition of *Aegle marmelos* fruit shell powder.[1]

Component	Bael fruit shell powder
Moisture (%)	11.83± 0.28
Ash (%)	1.66 ± 0.28
Protein (%)	7.53 ± 0.90
Fat (%)	3.13 ± 0.23
Fiber (%)	22.84.32 ± 1.27
Total carbohydrates (%)	53.01 ± 0.32

[1] Data is presented as means ± SD ($n = 3$).

3.2. Optimization of extraction of polysaccharide

3.2.1. Effects of ultrasonic conditions on extraction and polysaccharide yield

The yield of polysaccharides is greatly affected by various ultrasonication conditions. As depicted in Table 1B, to maximize polysaccharide powder yield, a range of different ultrasonic conditions were optimized. The influence of different independent variables on both extraction and polysaccharide yield is depicted in Fig. 1A and B. Across the examined parameters, including ultrasonic power, time, and solid-to-solvent ratio, the extraction yield ranged from 11.46 % to 17.91 %, while the polysaccharide yield varied from 9.45 % to 16.93 %. The impact of ultrasonic extraction power on both extraction and polysaccharide yield was examined across a range from 200 to 600 W. Fig. 1A and B reveal a significant increase in extraction and polysaccharide yield as the power increase from 200 W to 400 W ($P < 0.05$). This increase may be due to its direct influence on the cavitation phenomenon within the solvent, where cavitation collapse of microscopic bubbles under the influence of ultrasonic waves (Song, Liu, Umar, Ma, & Wang, 2023). These cavitation events generate localized high temperatures and pressures, resulting in physical and chemical effects such as shockwaves and shear forces, which aid in the breakdown of the solid matrix and facilitate the release of polysaccharides into the solvent. However, when the power exceeds 400 W, there is a gradual decline in extraction and polysaccharides yield with increasing power. This reduction could be due to the inefficiency of energy transmission into the medium at higher power, potentially due to the induction of an excessive number of bubbles during cavitation, hindering overall extraction efficacy (Chavan et al., 2022). Moreover, the yield of polysaccharides increased significantly as the time increased (up to 10 min), which could be due to the disruption of the cellular structure, leading to increased release and diffusion of the polysaccharides into the solvent (Wu et al., 2022). However, after a certain time (15 min), the extraction yield decreases slightly which may be due to the degradation of target

Table 1B
Experimental design for independent variables and the response of the extraction yield of *Aegle marmelos* fruit shell polysaccharides (AMFSP) in Box-Behnken design.

Runs	Ultrasonic power (W)	Time (min)	Solvent to solid (mg/mL)	Extraction yield (%)	Polysaccharide yield (%)
1	400	5	10	16.75	14.72
2	400	10	15	17.42	16.54
3	200	10	10	12.31	10.32
4	400	15	20	14.41	12.45
5	600	10	10	16.31	14.34
6	600	10	20	15.59	13.58
7	200	5.	15	11.46	9.45
8	400	5	20	15.18	13.14
9	400	10	15	17.39	16.03
10	600	5	15	15.61	13.59
11	600	15	15	15.01	13.09
12	**400**	**10**	**15**	**17.91**	**16.93**
13	400	15	10	14.65	12.69
14	200	15	15	12.82	10.85
15	200	10	20	13.01	11.05

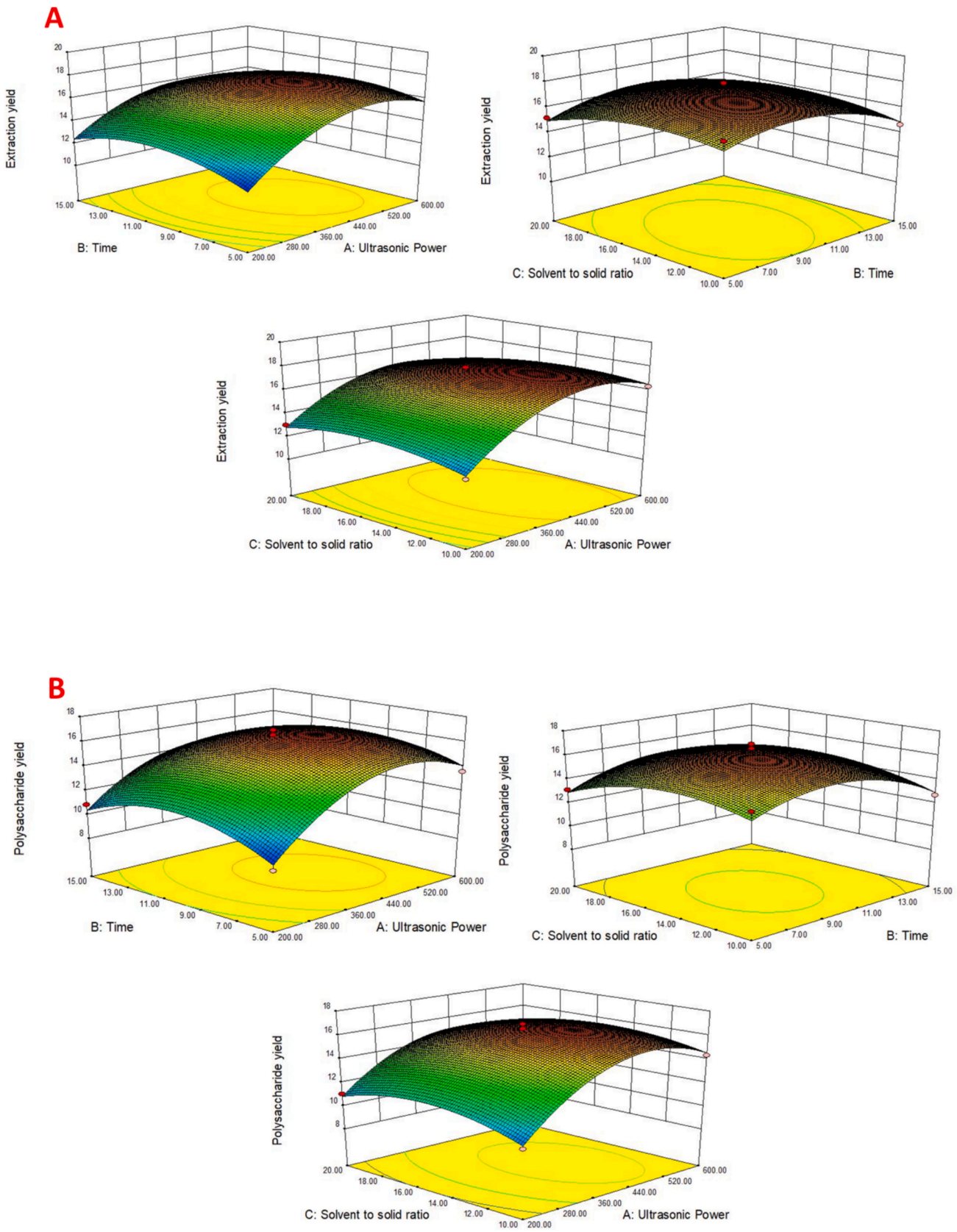

Fig. 1. Response surface plots (3D) showing the effects of ultrasonication conditions on (A) extraction yield (%) and (B) polysaccharides yield (%).

Table 1C
Analysis of variance for the ultrasonication extraction yield at three-level ultrasonic power (A), time (B), and Solvent-to-solid ratio (C).

Extraction yield						
Source	Sum of Squares	Mean df	Mean square	F Square	*P* value Prob > F	
Model	52.25	9	5.81	13.04	0.0057	**Significant**
A-Ultrasonic power	20.87	1	20.87	46.88	0.0010	
B-Time	0.56	1	0.56	1.25	0.3143	
C-Solvent to solid ratio	0.42	1	0.42	0.94	0.3767	
AB	0.96	1	0.96	2.16	0.2018	
AC	0.50	1	0.50	1.13	0.3359	
BC	0.44	1	0.44	0.99	0.3646	
A^2	21.19	1	21.19	47.60	0.0010	
B^2	7.79	1	7.79	17.51	0.0086	
C^2	2.81	1	2.81	6.32	0.0535	
Residual	2.23	5	0.45			
Lack of Fit	2.05	3	0.68	8.04	0.1127	**Not significant**
C·V (%)	4.43					
R^2	0.95					

Table 1D
Analysis of variance for the polysaccharide yield at three-level ultrasonic power (A), time (B), and Solvent-to-solid ratio (C).

Polysaccharide yield						
Source	Sum of Squares	Mean df	Mean Square	F Square	P value Prob > F	
Model	67.83	9	5.81	15.38	0.0039	**Significant**
A-Ultrasonic power	20.90	1	20.87	42.66	0.0013	
B-Time	0.41	1	0.56	0.85	0.4001	
C-Solvent to solid ratio	0.43	1	0.42	0.87	0.3930	
AB	0.90	1	0.96	1.84	0.2327	
AC	0.56	1	0.50	1.13	0.3358	
BC	0.45	1	0.44	0.92	0.3824	
A^2	29.81	1	21.19	60.84	0.0006	
B^2	13.52	1	7.79	27.60	0.0033	
C^2	6.59	1	2.81	13.46	0.0145	
Residual	2.45	5	0.45			
Lack of Fit	2.04	3	0.68	3.34	0.2388	**Not significant**
C·V (%)	5.28					
R^2	0.96					

compounds due to prolonged exposure to ultrasonic energy or saturation of the solvent with extracted solutes, which limits further extraction. Moreover, the polysaccharide yield exhibited a gradual increase as the solvent-to-solid ratio increased from 10 to 15 mL/g, followed by a decline from 15 to 20 mL/g. Increasing the water-to-raw material ratio improves the diffusion of materials across the cell membrane, facilitating quicker diffusion of polysaccharides (El Idrissi, Channab, Essamlali, & Zahouily, 2023). However, with further increases in the ratio, the density of the mixture decreases, leading to reduced efficiency in transferring ultrasonic energy. The results are consistent with those reported by Hu et al. (2022) who optimize the ultrasound-assisted extraction of coix seeds polysaccharides.

3.2.2. Model fitting

The extraction and polysaccharide yield data for each experimental run of bael fruit shell powder are provided in Table 1B. The statistical significance of differences in extraction efficiency and polysaccharide yield among various treatments were assessed using ANOVA with a 95 % confidence level, as presented in Tables 1C and 1D. Box-Behnken design (BBD) models effectively demonstrate the relationships in the data, showing significant regression and high R^2 values. Moreover, the models perfectly fit the data with a non-significant lack of fit for both response variables. The model's desirability was indicated as 0.758 as presented in Table 1E. Graphical representations for both responses were generated by simultaneously considering independent variables, accounting for their significance concerning the response. The equations for second-order regression coefficients for the extraction yield (0.95) and polysaccharide yield (0.96) of bael fruit shell powder are depicted in Eqs. (9) and (10), respectively.

$$\begin{aligned} \text{Y1 (Extraction Yield)} = {} & +17.57 + 1.61\,\text{A} - 0.26\,\text{B} - 0.23\text{C} - 0.49\,\text{AB} \\ & - 0.35\,\text{AC} + 0.33\,\text{BCE} - 2.40\,\text{A}^2 + 1.45\,\text{B}^2 \\ & - 0.84\,\text{C}^2 \end{aligned} \tag{9}$$

$$\begin{aligned} \text{Y2 (Polysaccharide Yield)} = {} & +16.50 + 1.62\,\text{A} - 0.23\,\text{B} - 0.23\text{C} \\ & - 0.47\,\text{AB} - 0.37\,\text{AC} + 0.33\,\text{BCE} \\ & - 2.84\,\text{A}^2 + 1.91\,\text{B}^2 - 1.34\,\text{C}^2 \end{aligned} \tag{10}$$

3.3. Characterization of polysaccharide

3.3.1. Monosaccharide composition

The High-performance liquid chromatography (HPLC) results revealed the monosaccharides composition of the AMFSP which include galactose (30.56 ± 0.76 %), galacturonic acid (24.72 ± 0.12 %), arabinose (17.26 ± 0.35 %), xylose (11.48 ± 0.21 %), glucose (10.52 ± 0.26 %), and rhamnose (5.39 ± 0.67 %) as presented in Fig. 2A. The monosaccharides constituents in the polysaccharides affect its functional properties. The high content of galactose and galacturonic acid, indicates its potential as a gelling agent and thickener in food products, as these sugars exhibit strong water-holding capacity, contributing to the texture and stability of food products (Ognyanov et al., 2020). However, the polysaccharides containing arabinose and galacturonic acid exhibit antioxidant properties. The antioxidant activity is attributed to the ability of these polysaccharides to scavenge free radicals, thus potentially offering

Table 1E
Desirability for optimization based on response surface methodology.

Constraints							
Name	Goal	Lower limit	Upper limit	Lower wight	Upper weight	Importance	
A-Ultrasonic power	minimize	200	600	1	1	3	
B-Time	minimize	5	15	1	1	3	
C-Solvent to solid ratio	minimize	10	20	1	1	3	
Extraction yield	maximize	11.46	17.91	1	1	3	
Polysaccharide yield	maximize	9.45	16.93	1	1	3	
Solutions							
Number	**Ultrasonic power**	**Time**	**Solvent to solid ratio**	**Extraction yield**	**Polysaccharide yield**	**Desirability**	
1	387.57	6.78	10.70	16.726	15.096	0.758	Selected

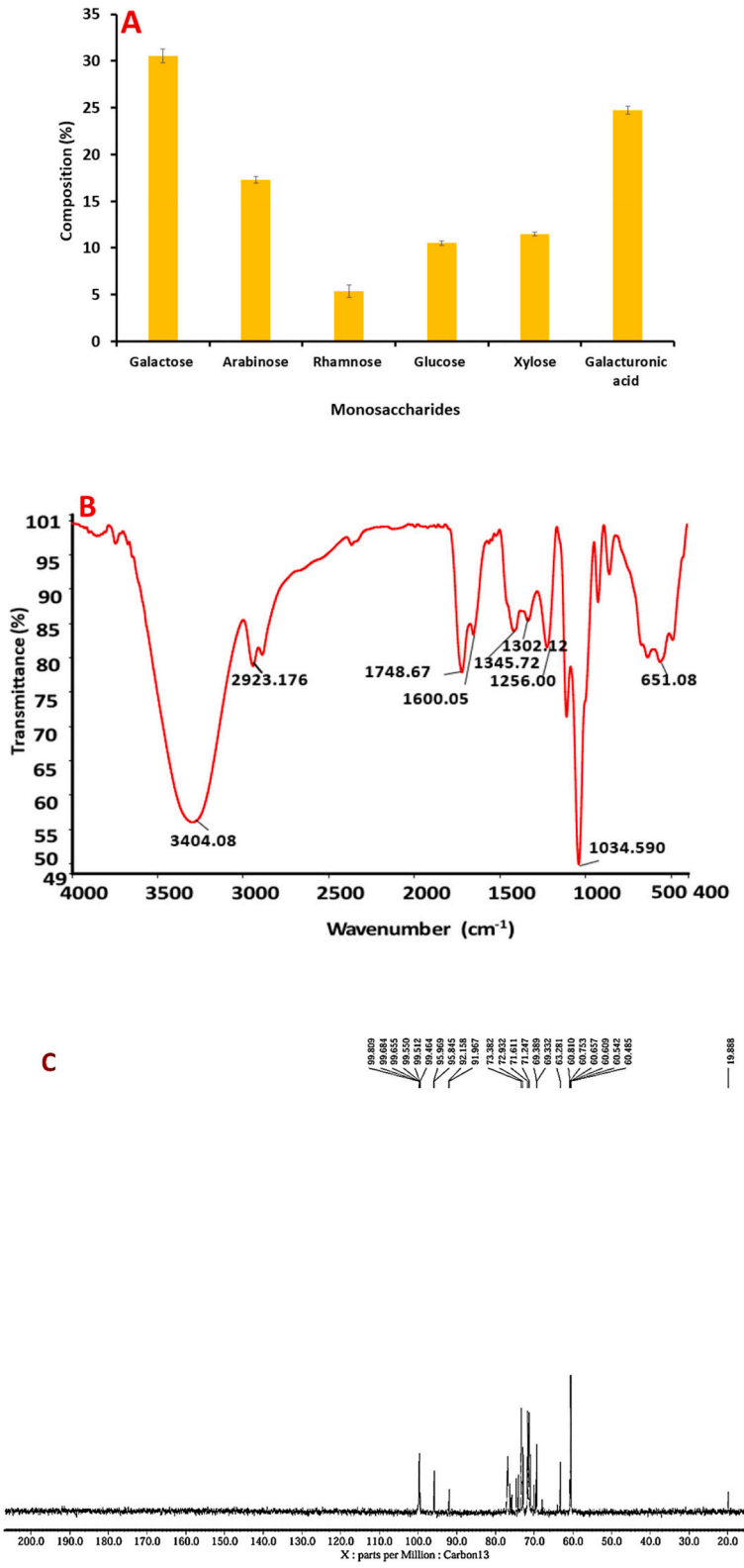

Fig. 2. Characterization of AMFSP using different analytical techniques: (A) monosaccharides composition, (B) Fourier transform infrared spectroscopy, (C) Nuclear magnetic resonance (D) DSC thermograph, (E) TGA thermograph, (F) particle size distribution, (G) zeta potential, (H) scanning electron microscopy, and (I) X-ray diffraction. AMFSP; *Aegle marmelos* fruit shell polysaccharide.

protective benefits against oxidative stress-related diseases (Yang et al., 2021). Moreover, arabinogalactan may enhance the emulsifying capability of the polysaccharides primarily attributed to the presence of arabinogalactan protein. Likewise, similar concentrations of monosaccharides were found by (Shiyang Zhou & Huang, 2023) for the *Juglans regia* shell polysaccharides. Overall, the monosaccharide composition of AMFSP plays a significant role in determining its physicochemical properties and potential biological activities.

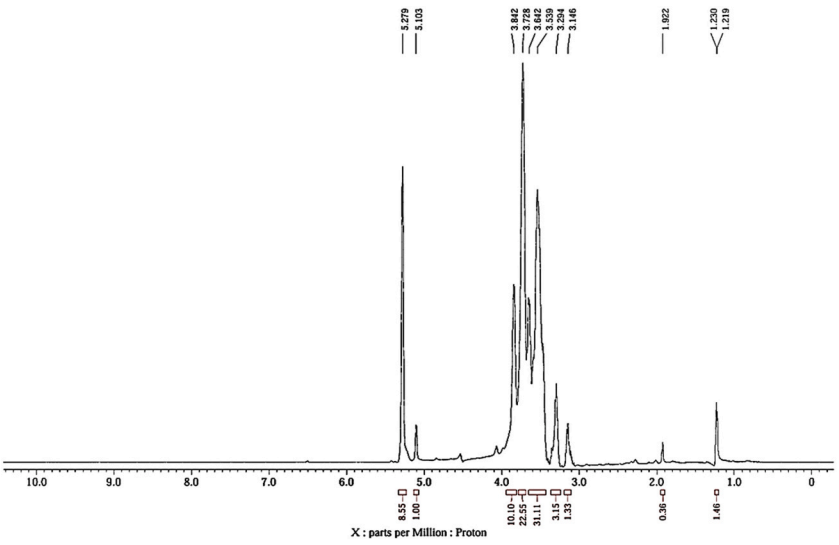

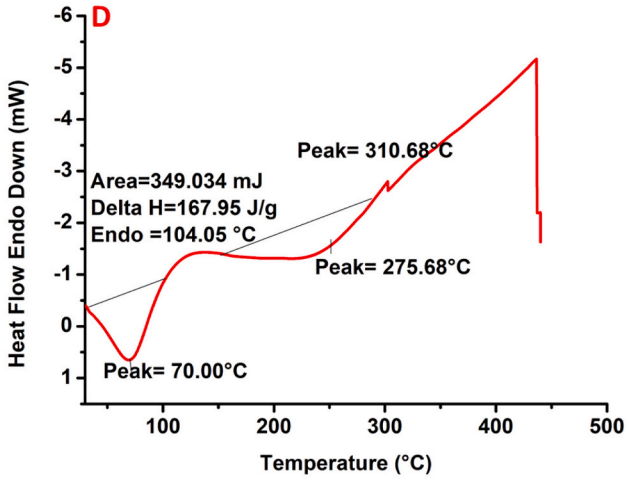

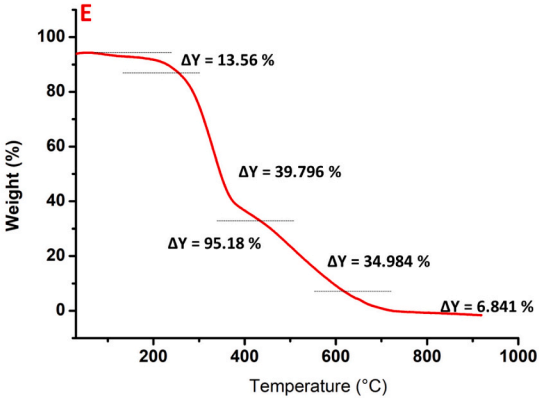

Fig. 2. (*continued*).

3.3.2. *Fourier transform infrared spectroscopy*

The FTIR spectrum of AMFSP revealed its several characteristic absorption peaks indicative of its functional groups and molecular structure as shown in Fig. 2B. The prominent peak at 3404.08 cm^{-1} is typically associated with the stretching vibrations of hydroxyl (O—H) groups, a common feature in polysaccharide structures due to the presence of alcohol groups (Muhammad et al., 2020). The sharp peak at 2923.17 cm^{-1} can be attributed to the stretching of aliphatic C—H bonds, likely from methylene groups, which are a backbone feature in many organic compounds (Hashim et al., 2024). The peak at 1748.67 cm^{-1} suggests the presence of carbonyl (C═O) functional groups, possibly from carboxylic acids or esters. The absorption bands near 1600.05 cm^{-1} may indicate N—H bending vibrations, which are characteristic of amides, suggesting the presence of proteinaceous material or amino sugars

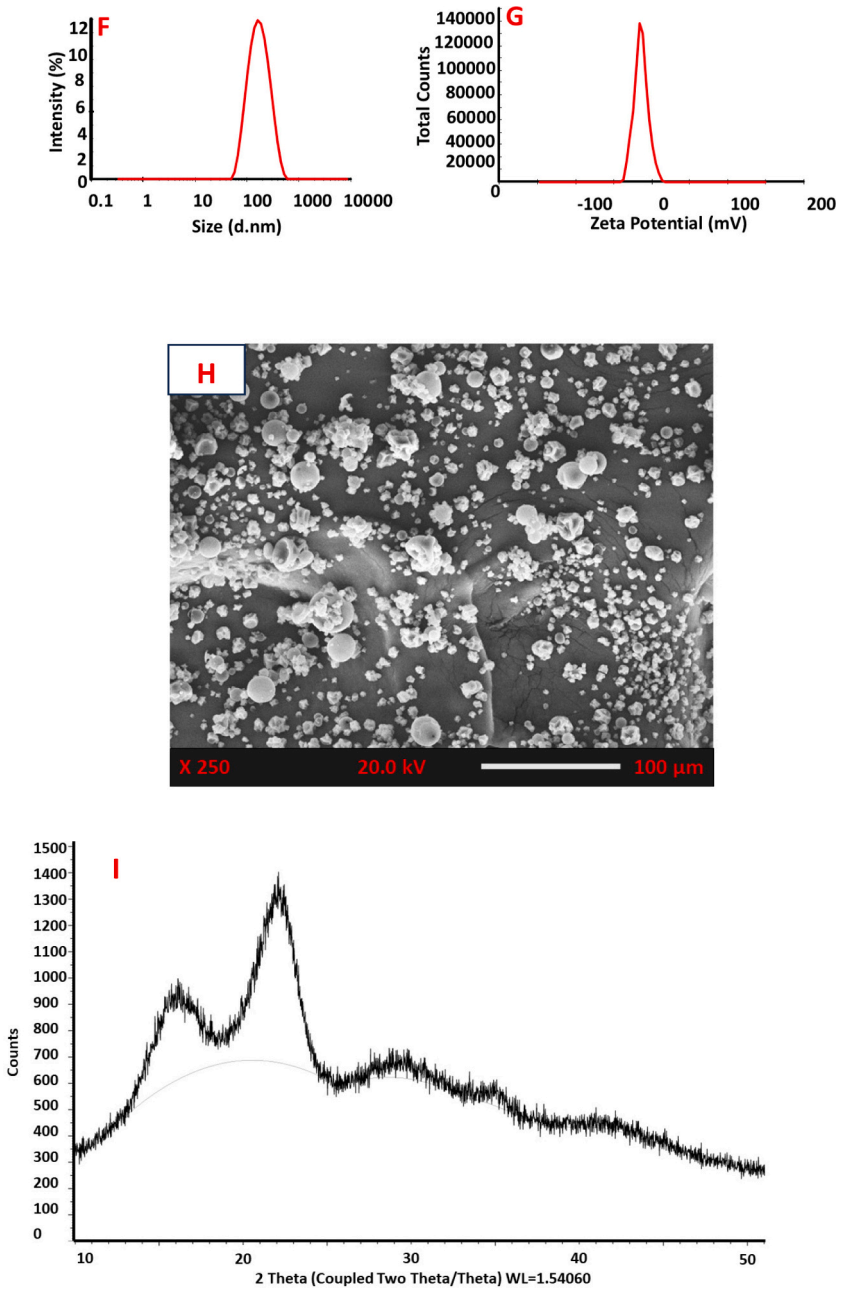

Fig. 2. (*continued*).

within the polysaccharides (Yu et al., 2022). The medium bands around 1345.72 cm^{-1} are indicative of the bending vibrations of CH_3 and CH_2 groups, which align with the aliphatic character of the polysaccharides. Peaks at 1302.12 and 1256.00 cm^{-1} are associated with C—O stretching, a characteristic motion within carbohydrate molecules, while the strong peak at 1034.59 cm^{-1} suggested C—O—C stretching vibrations of glycosidic linkages, confirming the polysaccharide nature of the sample (Hong et al., 2021). Finally, the peak at 651.08 cm^{-1}, may suggest the presence of specific structural features, such as crystalline regions or unique bending modes, that may influence the material's properties. A similar result was obtained by (Feng et al., 2023) for the FTIR spectra of polysaccharides extracted from *Camellia oleifera* fruit shell. Overall, these spectral features provide insight into the intricate molecular architecture of AMFSP and can be pivotal in determining its potential for various applications based on its functionality.

3.3.3. Nuclear magnetic resonance analysis

1D NMR, including both ^{1}H and ^{13}C NMR, is commonly used in the characterization of polysaccharides. The α- or β-configuration of the anomeric proton (H1) and anomeric carbon (C1) in sugar residues can be identified in the ^{1}H and ^{13}C NMR spectra, as demonstrated in Fig. 2C. The prominent peaks between 99.80 and 91.96 ppm correspond to the anomeric carbons of glucose and xylose rings, suggesting the presence of β (1 → 4) glycosidic linkages, where the C1 of one sugar is bonded to the C4 of another. The multiple peaks between 73.38 and 69.38 ppm are attributed to carbonyl (C═O) carbons from carboxylic acid (—COOH) groups, indicating the presence of galacturonic acid. The peak at 63.28 ppm is associated with methylene carbons (C—C) in arabinose and mannose, reflecting β (1 → 6) glycosidic bonds between sugar units. Additionally, the peak at 60.75 to 60.48 ppm points to the presence of methoxy (—OCH_3) groups in rhamnose, confirming the occurrence of rhamnogalacturonan in the plant mucilage. A distinct peak at 19.88 ppm indicates the presence of methyl groups in galactose and rhamnose,

linked to the sugar backbone through glycosidic bonds.

The ^{1}H NMR spectrum of the mucilage also provides detailed information about the proton as shown in Fig. 2C. The signals observed in the range 5.27–5.10 ppm could be assigned to protons attached to carbon atoms positioned nearby to glycosidic bonds (e.g., anomeric position). The aliphatic region (3.84–3.14 ppm) is associated with methylene (CH_2) or methine (CH) groups within the sugar moieties. A signal at 1.92 ppm in the alkyl region corresponds to protons in methyl (CH_3) groups or other aliphatic environments, and additional signals in the range of 1.23–1.21 ppm confirm the presence of protons in methyl groups. The methyl groups resonating at 1.19 ppm and 1.96 ppm are specifically attributed to rhamnose, while protons linked to C-6 of galactose resonate at 3.65 ppm and 3.70 ppm, and those linked to C-4 of galactose appear at 3.98 ppm and 4.28 ppm. In conclusion, the combined analysis of ^{13}C and ^{1}H NMR spectra provides a comprehensive molecular characterization of the mucilage. The ^{13}C spectrum identifies key carbon functional groups, confirming the presence of sugars such as glucose, xylose, galactose, galacturonic acid, arabinose, and rhamnose. The ^{1}H spectrum reveals specific proton environments, highlighting aromatic compounds, methylene groups in sugar units, and methyl groups linked to various sugars.

3.3.4. Differential scanning calorimetry

As presented in Fig. 2D, the DSC thermogram for AMFSP exhibits a notable endothermic peak at 70.00 °C, which is indicative of a phase transition, possibly the melting point of the polysaccharides or a dehydration process where bound water is being lost. The enthalpy change of 167.95 J/g associated with this peak is significant, as it quantifies the energy absorbed by the sample during this transition, suggesting strong hydrogen bonding between water molecules and the polysaccharide chains. The endothermic event concludes at 104.05 °C, indicating that the polysaccharides maintain their structural integrity up to this temperature (Surya et al., 2023). After this temperature, the DSC curve shows a steady increase in heat flow, which may suggest the beginning of thermal degradation or other complex exothermic reactions such as oxidative stability. This increase in heat flow indicates the material's response to further thermal stress, potentially leading to the breakdown of the polysaccharide chains (Hill et al., 2021). The area under the endothermic event, measured at 310.68 mJ, provides a quantitative measure of the total energy absorbed, which could be correlated with the moisture content and thermal stability of the polysaccharides. Our results correspond to the research conducted by (Mohammed et al., 2020) for the polysaccharides extracted from *Medemia argun* fruit. The thermogram suggests that the utilization of AMFSP may be advantageous in applications that do not exceed the identified temperature thresholds, thereby ensuring functionality.

3.3.5. Thermogravimetric analysis

The TGA curve of AMFSP demonstrates a characteristic thermal degradation pattern, as presented in Fig. 2E. The initial minor weight loss below 100 °C can be attributed to the evaporation of moisture content within the AMFSP. This phase is typically associated with the loss of physically adsorbed water and some volatile compounds (Li et al., 2020). The relatively stable weight before this temperature suggests that AMFSP is thermally stable in this lower temperature range. As the temperature increases beyond this point, a significant weight loss is observed, which is the primary degradation phase. This sharp decline, which results in a ΔY of 95.18 %, indicates the breakdown of the main polysaccharide structure. This large-scale decomposition is likely due to the pyrolytic breakdown of the glycosidic linkages in the polysaccharides, leading to the formation of monosaccharides and other volatile products (Chen et al., 2023). The temperature at which the rapid weight loss begins is a critical parameter, as it signifies the onset of thermal decomposition. The rate of weight loss appears to slow down as the temperature approaches 918.6 °C, suggesting the approach towards a residual mass. This residual mass could be composed of carbonaceous material and inorganic ash, which are non-volatile remnants of the thermal decomposition of AMFSP. In conclusion, the TGA analysis of AMFSP has revealed valuable insights into its thermal stability and decomposition behavior.

3.3.6. Particle size and zeta potential

The particle size distribution of the AMFSP was evaluated using the dynamic light scattering technique which was found to be 142.3 ± 1.24 nm with a polydispersity index of 0.34 as shown in Fig. 2F. The particle size could be attributed to various factors, including sources, extraction processes, and the inherent nature of polysaccharides. These factors may influence the formation of polysaccharide aggregates or clusters, leading to the variability in particle size (Dong et al., 2024). The surface charge of the AMFSP was determined as −25.52 ± 1.02 mV as presented in Fig. 2G. The measured zeta potential indicates the potential for colloidal stability and instability (Pochapski et al., 2021). The higher zeta potential value is indicative of the electrostatic repulsion between particles, resulting in improved colloidal stability and reduced aggregation. Comparable findings have been reported by Purwandari, Westerbos, Lee, Fogliano, & Capuano (2023) for polysaccharides. Overall, the consistent particle size and stable dispersion are the key factors for the product quality.

3.3.7. Scanning Electron Microscopy (SEM)

The SEM analysis of spray-dried AMFSP is represented in Fig. 2H, which revealed a heterogeneous distribution of particles varying in size, with both smooth spherical and irregularly shaped rough particles present. The observed surface texture and aggregation indicate a mixture of different morphological forms resulting from the spray drying process (Nadendla et al., 2024). Notably, there is evidence of particle aggregation, where smaller particles cluster together to form larger conglomerates. This aggregation is likely due to the inherent stickiness of polysaccharides and the conditions of the drying process. Additionally, particle shrinkage was noted, a phenomenon frequently encountered in spray drying as a result of rapid water evaporation (Hassanbeiki et al., 2024). The shrinkage can result in the formation of denser, more compact particles with reduced volume. No research has yet been conducted on the spray drying of AMFSP; however, similar results were found in the spray drying of psyllium and okra mucilage (Mohammad et al., 2024). Overall, the variation in particle size and morphology, is crucial for applications where particle characteristics influence behavior, such as in drug delivery systems where controlled release rates are important. Applications such as emulsifiers or stabilizers in foods could benefit from the rough and textured surfaces' enhanced effectiveness due to the increment surface area that allows for better interaction with other components.

3.3.8. X-ray diffraction

The XRD pattern of the polysaccharide extracted from the *Aegle marmelos* fruit shell is shown in the Fig. 2I. The diffraction pattern detects distinct peaks indicating the presence of crystalline regions within the polysaccharide. The major peak is observed at a 2θ value of approximately 22°, which can be associated with the regular arrangement of polysaccharide chains in a crystalline lattice. In addition to the crystalline peaks, there is a broad peak in the range of 10°–20°, demonstrating the presence of an amorphous region. This is characteristic of many polysaccharides, which typically exhibit a combination of crystalline and amorphous domains. The crystallinity can impact the physical properties of the polysaccharide, such as its mechanical strength and thermal stability. Moreover, amorphous regions are typically more flexible and less dense compared to crystalline regions which contribute to the material's solubility and reactivity (Tamo, 2024). The presence of both crystalline and amorphous regions is consistent with the typical behavior of polysaccharides, which often have semi-crystalline structures due to the presence of ordered and disordered domains. In similar research, the polysaccharide extracted from *Ocimum*

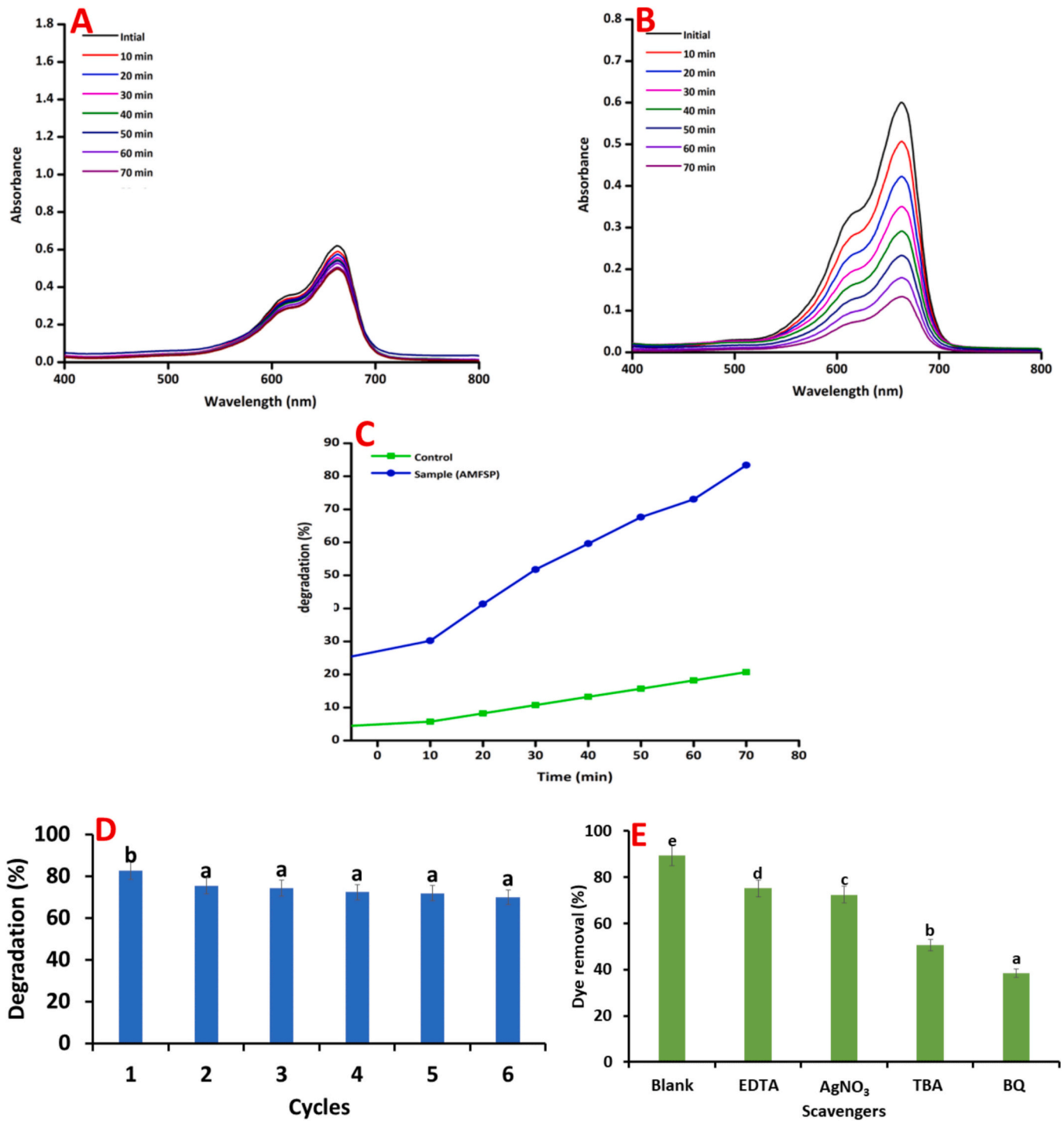

Fig. 3. Photocatalytic dye degradation of methyl green under irradiation of UV light (A) Control, (B) using AMFSP, (C) % degradation of methyl green dye, (D) Reusability of AMFSP catalyst, and (E) Removal of methyl green dye using AMFSP in the presence of different scavengers.The results were expressed as the mean ± standard deviation of ≥3 independent replicates and error bars represent the standard deviation from the mean values, while different lowercase (a–b) and (a–e) letters above each bar represent significantly different values based on analysis of variance (ANOVA) and post hoc tests.AMFSP; *Aegle marmelos* fruit shell polysaccharides, benzoquinone (BQ), ethylenediaminetetraacetic acid (EDTA), tertiary butyl alcohol (TBA), and silver nitrate (Ag NO_3). (For interpretation of the references to color in this figure legend, the reader is referred to the web version of this article.)

album L. seed displayed semi-crystalline biopolymer with major crystalline reflections at 15.94, 22.67, and 29.36 (Arab et al., 2021). Thus, this structural characteristic is crucial for determining its physical properties and potential applications in various fields.

3.4. Photocatalytic dye reduction

The absorption spectra of a dye solution over time, under the influence of an AMFSP photocatalyst, in comparison to the control, are depicted in Fig. 3A and B, and photocatalytic dye reduction efficiency of control and AMFSP are shown in Fig. 3C. The polysaccharides were

found to be very effective in the reduction of methyl green dye (82.79 ± 0.39 % in 70 min) as compared to the control (19.98 ± 0.39 % in 70 min). The lack of observed spectral changes and the low degradation efficiency revealed that the dye degradation process was highly inefficient without a catalyst. The nano-size particles of the AMFSP possess a high surface area-to-volume ratio, resulting in an increased number of active sites available for chemical reactions. Moreover, upon exposure to UV light irradiation, the polysaccharide catalyst absorbs photons, leading to the generation of electron-hole pairs (Gao, Yin, Li, et al., 2023; Kumar et al., 2020). These photoinduced electron-hole pairs participate in redox reactions with the dye molecules adsorbed onto the surface of the polysaccharide catalyst. The electrons (e−) interact with oxygen molecules (O_2), resulting in the formation of superoxide radicals ($\bullet O^{-2}$), whereas the holes (h+) react with water molecules (H_2O), producing (•OH) hydroxyl radicals (Liu et al., 2021). Both superoxide and hydroxyl radicals are highly reactive species capable of oxidizing the dye molecules, thereby breaking down their chemical structure and leading to decolorization.

The degradation kinetics of catalysts revealed that the degradation rate remained constant over time, suggesting a linear correlation with time ($R^2 = 0.9947$). The kinetics of dye degradation were observed to follow a pseudo-first-order model, indicative of the catalytic efficiency of AMFSP. The significant decrease in dye absorbance at the maximum wavelength highlights the ability of the polysaccharide catalyst to facilitate the breakdown of dye molecules under UV light irradiation (Pandey et al., 2020). The findings of this study align with the results reported by (Pandey et al., 2020) for the catalytic degradation of dyes using carrageenan-stabilized nanoparticles. Overall, the combined action of photoinduced electron-hole pairs and reactive oxygen species contributes to the effective degradation of dyes by AMFSP under UV light irradiation. In addition, the reusability of AMFSP was evaluated by monitoring the photocatalytic degradation rate of the catalyst after each cycle. When comparing the performance it became evident that AMFSP exihibited notably better stability after six cycle. In the first cycle, it showed a dye degradation rate of 82.79 ± 0.39 % that only decreased to 70.02 ± 1.32 % by the sixth cycle as shown in Fig. 3D. This presents that the AMFSP photocatalyst remains stable after six successive reuse cycles with minor loss in photocatalytic efficiency.

3.4.1. Scavenging activity

The removal efficiency of methyl green dye using AMFSP in the presence of various scavengers was evaluated, as presented in Fig. 3E. The results detected that EDTA exhibited radical scavenging (75.12 ± 1.34 %), $AgNO_3$ showed electron transfer interference (72.46 ± 0.98 %), TBA showed hydroxyl radical scavenging (50.67 ± 1.56 %), and BQ showed superoxide radical scavenging (38.46 ± 1.37 %), compared to the blank (89.42 ± 1.71 %). EDTA was utilized to counteract the hole (h+) which indicating the significant role of photogenerated holes, however, $AgNO_3$, was utilized for capturing the free electrons, indicating the involvement of photogenerated electrons. On the other hand, TBA, eliminates the hydroxyl radicals, while benzoquinone (BQ) was used to neutralize the superoxide free radical (Gao, Yin, Guo, et al., 2023). The significant reduction in dye removal efficiency in the presence of different scavengers indicates the involvement of multiple reactive species in the photocatalytic degradation of methyl green dye. The results suggest the following order of reactive species contribution to the degradation process: superoxide radicals (O2•−) > hydroxyl radicals (•OH) > photogenerated holes (h+) > photogenerated electrons (e−). The substantial impact of BQ on the dye removal efficiency indicates that superoxide radicals play a dominant role in the photocatalytic process, likely due to their efficient generation and subsequent reactions with dye molecules (Yan et al., 2024). The notable reduction in degradation efficiency with TBA further emphasizes the importance of hydroxyl radicals, known for their high oxidative potential. The involvement of photogenerated holes and electrons is also evident from the reduced efficiency with EDTA and $AgNO_3$, respectively, suggesting that these species participate in initiating and propagating the degradation reactions. Overall, the photocatalytic degradation of methyl green dye using AMFSP is a complex process involving multiple reactive species, with superoxide radicals and hydroxyl radicals playing significant roles in achieving effective dye removal.

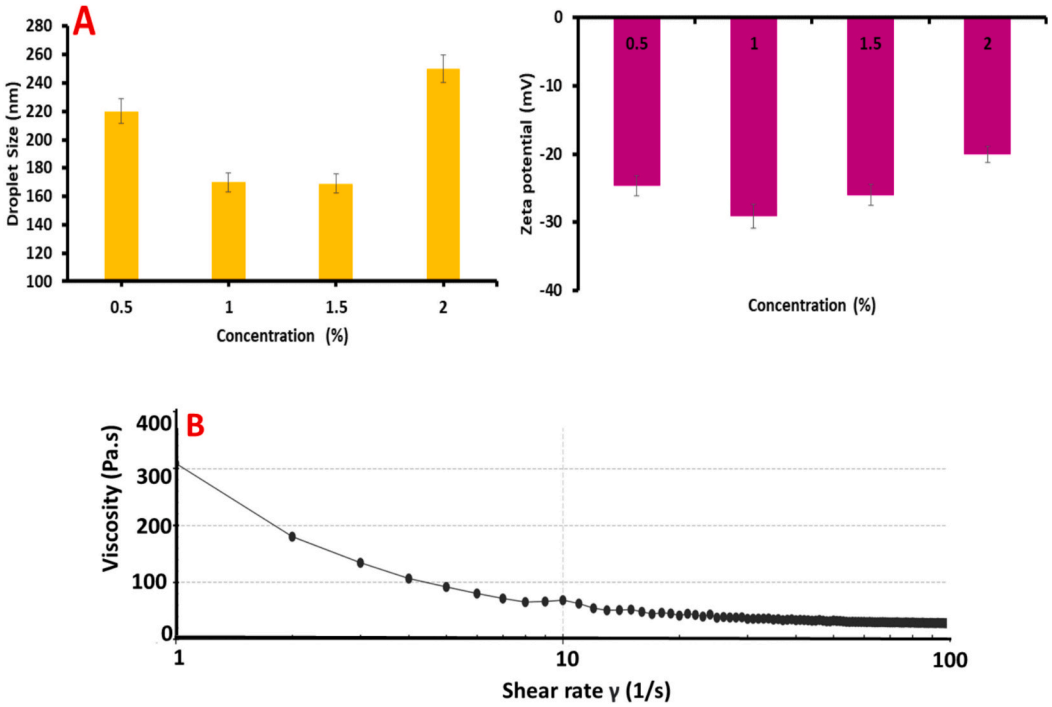

Fig. 4. Optimization of coating solution based on (A) droplet size and zeta potential and (B) Shear viscosity.

3.5. Optimization of coating solution

The coating solutions (0.5, 1, 1.5, and 2 %) were optimized based on their particle size (220–250 nm) and zeta potential (−29 to −20 mV) as shown in Fig. 4A. At a lower concentration of 0.5 % w/v, the particle size observed was 220 ± 0.62 nm with a zeta potential of −24 ± 0.23 mV, resulting in a stable coating solution. As the concentration increased to 1 % w/v, both particle size and zeta potential improved to 170 ± 0.54 nm and −29 ± 0.14 mV, respectively, indicating enhanced stability due to optimal repulsion forces that prevent particle aggregation (Sun et al., 2021). Further increased the concentration to 1.5 % w/v resulted in a continued decrease in particle size to 169 ± 0.51 nm and a slightly reduced zeta potential of −26 ± 0.73 mV, maintaining system stability. The decrease in particle size with increasing concentration up to 1.5 % w/v suggests that higher concentrations of AMFSP facilitate better dispersion and more uniform distribution of particles within the solution. The zeta potential values, which remain negative across all concentrations, point out that the particles are negatively charged (Trenkenschuh & Friess, 2021). The most negative value observed at a concentration of 1 % w/v (−29 ± 0.14 mV) correlates with the highest stability among all formulations. This is because high absolute zeta potential values indicate strong electrostatic repulsion forces among the colloidal particles, which effectively counteract the natural tendency for aggregation, thereby enhancing stability (Pochapski et al., 2021). However, at the highest concentration of 2 % w/v, particle size enhanced to 250 ± 0.23 nm, and zeta potential decreased to −20 ± 0.12 mV, suggesting a reduction in stability. This change is attributed to increased particle aggregation and reduced electrostatic repulsion between particles. In conclusion, the 1 % w/v was the optimal AMFSP concentration for coating applications, where the balance between particle size reduction and zeta potential maximization results in a stable and homogenous solution.

3.5.1. Rheology of coating solution

The rheological properties of coating solutions (1 % w/v) were investigated, and results are presented in Fig. 4B The apparent viscosity decreased with increasing shear rate, indicating its non-Newtonian behavior within the range of 1–50 s^{-1}. Initially, at zero shear and low shear rates, the viscosity was higher due to the entanglement of the polysaccharides chain. As the shear rate rose, the number of entanglements diminished, leading to non-Newtonian behavior. Moreover, at higher shear rates (50–100 s^{-1}), the apparent viscosity stabilized, showing a Newtonian behavior which may be due to the disentanglement of the polysaccharides chain. The viscosity decreased with increasing shear rates, demonstrating shear-thinning behavior, which is advantageous for coating applications due to its facilitation of easier application and uniform coverage. The molecular weight, concentration, and type of polysaccharide in the solution, may influence these rheological properties. (Shen et al., 2022) also observed the similar rheological characteristics of *Panax notoginseng* polysaccharides and concluded that the concentration of polysaccharides did not exert a significant influence on viscosity.

3.6. Physiochemical properties of cut fruits

3.6.1. Color

As depicted in Fig. 5A, the polysaccharide coating effectively reduces the decline in lightness (L*) of fresh-cut apples, maintaining a higher value throughout the storage period. While both coated (64.71 ± 0.60 to 52.13 ± 0.70) and control samples (64.11 ± 0.37 to 33.59 ± 0.2) experienced a decrease in L* values, coated apples demonstrated a significantly slower rate of decline, indicating better lightness preservation. This suggests that the coating may provide a barrier against factors that contribute to the loss of lightness, such as moisture loss and enzymatic browning (Maringgal et al., 2020). The a* values decreased for both groups over time; however, this decrease was more controlled in coated apples (60.53 ± 0.4 to 53.64 ± 0.5). The slower decrease in a* values for coated fresh-cut apples indicates the minimal biochemical alterations in the fruits, consequently leading to a delayed ripening process, possibly due to the antioxidant properties of the polysaccharide coating that inhibit oxidative changes and hence increase the shelf life of fresh-cut apples (Ali et al., 2022). Both coated and control exhibited a decrease in b* values, the values of control decreased from 7.95 ± 0.61 to 3.39 ± 0.60, while the values of treated group showed a slightly lesser decline from 7.99 ± 0.18 to 5.85 ± 0.90. This suggests the coating's protective effect against yellow color loss, possibly related to its ability to retain moisture and thereby slow down degradation and enzymatic browning processes. The results are in line with the study of (Jung & Choi, 2021) for apple fruit coated with natural monoesters.

As shown in Fig. 5B, the color difference (ΔE) analysis showed that

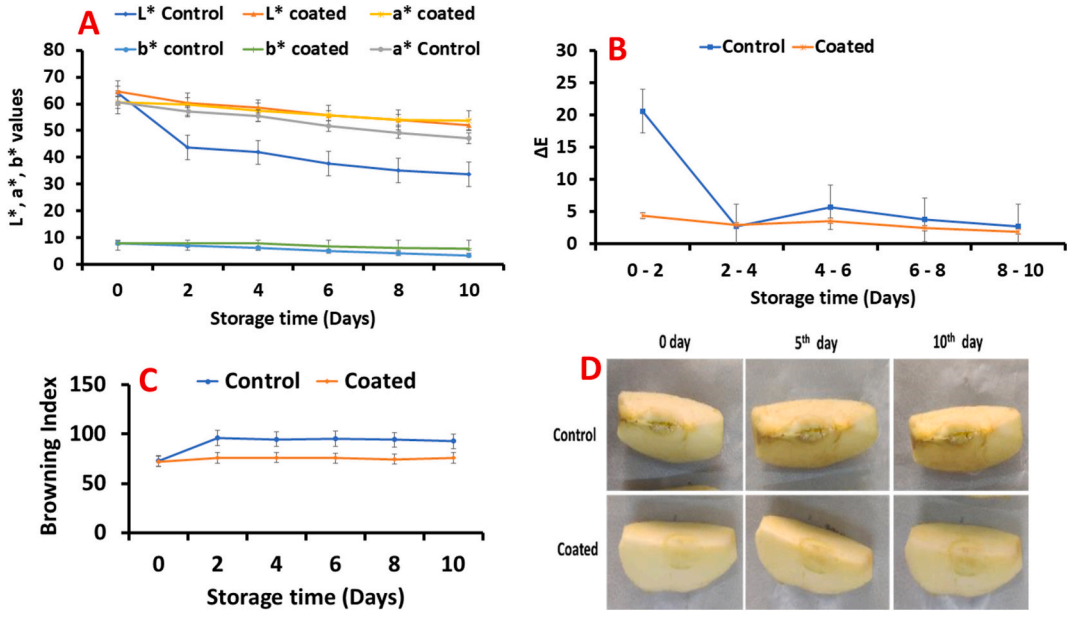

Fig. 5. Color characteristics of control and coated fresh-cut apple at 4 °C. (A) L*, a*, b* values (B) Color differences (ΔE), (C) Browning Index, (D) The apparent morphology fresh-cut apple slices during storage.

the control apples experienced a significant color change during the initial storage period (0–2 days), with a ΔE of 20.62, indicating rapid degradation, likely due to enzymatic browning. In contrast, the coated apples exhibited a much lower ΔE of 4.39 in the same period, demonstrating the effectiveness of the coating in delaying browning. During storage, the coated apples consistently showing smaller changes while, control apples continued to exhibit significantly more color differences. Beyaz et al. (2010) revealed that the browning index is more specific to brown coloration compared to the total color difference (ΔE), as ΔE does not reflect the direction of the color change. The ΔE can also be

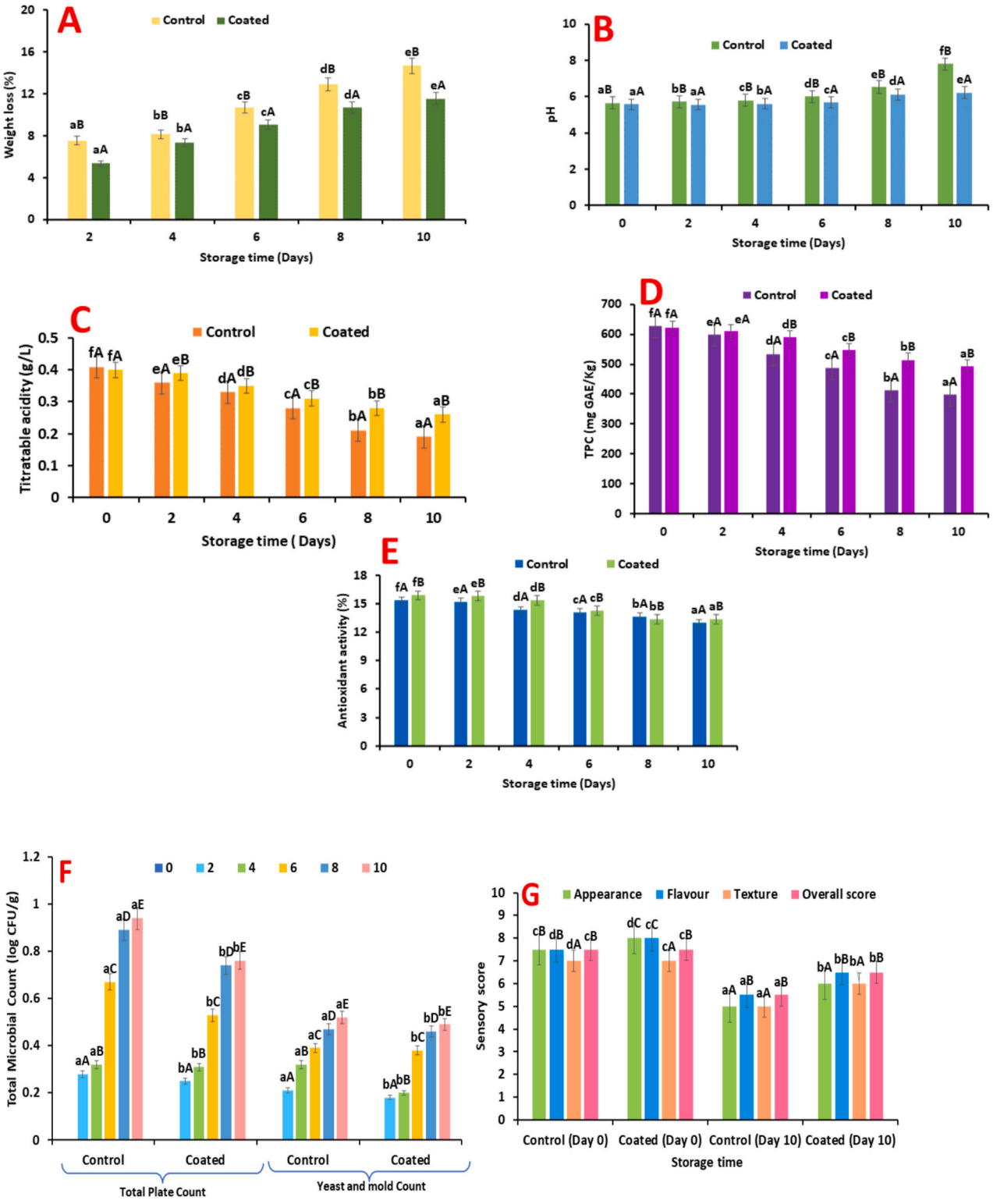

Fig. 6. Physico-chemical characteristics of coated apple fruit at 4 °C. (A) weight loss, (B) pH, (C) titratable acidity, (D) total phenolic content, (E) antioxidant activity, (F) total microbial count, and (G) sensory evaluation. The results were expressed as the mean ± standard deviation of ≥3 independent replicates and error bars represent the standard deviation from the mean values, while different lowercase (a–f) and uppercase (A–E) letters above each bar represent significantly different values within the storage time (days) and treatments, respectively, based on analysis of variance (ANOVA) and post hoc tests.

influenced by other color changes, such as the coloration from anti-browning agents used during apple treatment. Typically, increased enzymatic browning activity corresponds to higher ΔE values. However, ΔE does not consistently align with enzymatic browning activity.

The browning index is an indicator of quality deterioration in fruits, representing the extent of enzymatic browning and overall visual appeal. The browning index of both the samples increased during storage (Fig. 5C). On day 0, both control and coated fresh-cut apples had similar indices, with the control at 72.57 and the coated at 72.08. However, the browning of the control sample (92.69) increased significantly over the days during the storage. In contrast, the coated apples showed a non-significantly (75.64) difference in the browning throughout the storage period. The apparent morphologyof fresh-cut apple slices during storage is given in Fig. 5D. This highlights the coating's effectiveness in significantly slowing the browning process and preserving the visual quality of the fruit over time (Arnold & Gramza-Michałowska, 2022). Similar trend has been obtained by Shrestha et al. (2020) for controlling the browning and enzymatic activity on fresh-cut apple slices. Overall, the effectiveness of bael fruit shell polysaccharide coating in preserving the color quality of apples is attributed to its potential antioxidant properties and its physical barrier effect, which slows down oxidative reactions and enzymatic browning.

3.6.2. Weight loss, pH, and acidity

The weight loss of the fresh-cut apples is presented in Fig. 6A and observed an increase in weight loss for both control and coated samples over time. However, the rate of weight loss is consistently lower in the apples coated with bael fruit shell polysaccharides (11.55 ± 0.45 %) compared to the control group (14.66 ± 0.31 %). The results suggest that the coating of AMFSP effectively reduces the weight loss in apples over time which may be due to the polysaccharide coating's ability to act as a barrier to moisture loss that contributes as a primary factor in the weight loss of fresh produce (Zhai et al., 2020). The hydrophilic nature of polysaccharides helps in retaining moisture within the fruit, thus reducing the rate of weight loss (Kocira et al., 2021). On the other hand, the pH of the both control and coated samples increased during storage as shown in Fig. 6B, which may be due to respiration and enzymatic activity within the fresh-cut apples. The control samples (7.8 ± 0.18) showed a significant increase ($p > 0.05$) in the pH and a gradual increase was observed in coated samples (6.23 ± 0.76) on the 10th day of storage. The rise in pH level can be attributed to the fruit ripening and senescence. This leads to a reduction in the fruit's acid content, as acids act as substrates for the respiratory metabolism (D. Wang et al., 2021). As the rate of metabolic respiration increases, the acidity of the fruit tends to decline. The titratable acidity of both the samples was presented in Fig. 6C which was (control, 0.41 ± 0.12 g/L and coated, 0.40 ± 0.15 g/L) decreased during storage. The titratable acidity of the control sample (0.19 ± 0.23 %) was decreased significantly ($p < 0.05$) as compared to the coated samples; (0.26 ± 0.19 %) on the 10th day of storage. The acidity of the fruits is primarily influenced by the rate of metabolism due to respiration and the presence of organic acids. Similar results have been reported by Tosif et al. (2023) for the apple coated with *aloe vera* and carboxymethyl cellulose binary blend.

3.6.3. TPC

The total phenolic content for both the coated and control apples was measured at 0, 2, 4, 6, 8, and 10 days. The results are presented in Fig. 6D. Initially, the phenolic content values were similar between the coated (622.55 ± 0.45 mg GAEkg^{-1}) and control (627.66 ± 0.12 mg GAEkg^{-1}) apples. However, on day 12th, the phenolic content of the coated apples was 492.27 ± 0.34 mg GAEkg^{-1}, while the control apples decreased to 398.22 ± 0.41 mg GAEkg^{-1}. During storage time, the polyphenolic acid content of both coated and uncoated apples decreases, with the control samples showing a more pronounced decline. This may be due to the polysaccharide coating that forms a physical barrier and limits the diffusion of oxygen and moisture, thereby reducing enzymatic browning and oxidative degradation, which are common causes of polyphenolic acid loss in fruits (Riaz et al., 2021). Moreover, the bael fruit shell polysaccharides coating may have a protective effect on the polyphenolic acids, slowing down their degradation compared to the control. Similar results were found by (Solís-Contreras et al., 2021) for the apple fruit coated with bioactive compounds combined with cinnamon essential oil. In conclusion, the results suggest that coating fresh-cut apples with bael fruit shell polysaccharides may help preserve polyphenolic acids to some extent compared to uncoated apples, potentially offering a means of extending the shelf life and enhancing the nutritional value of the fruit.

3.6.4. Antioxidant analysis

The antioxidant activity was decreased over storage in both coated (15.87 ± 0.23 to 13.37 ± 0.32 %) and control sample (15.33 ± 0.23 to 12.99 ± 0.12 %) as presented in Fig. 6E. This reduction could be due to the degradation of polyphenolic compounds, which are major contributors to antioxidant activity in fruits. Despite the decline, the coated apples generally maintained higher levels of antioxidant activity compared to the control group throughout the observation period. This suggests that the bael fruit shell polysaccharides coating may have a protective effect on the antioxidants present in the apples, potentially slowing down their degradation compared to the control group (Solís-Contreras et al., 2021). The polysaccharide coating may provide a physical barrier against environmental factors such as oxygen, light, and moisture, which can promote the degradation of antioxidants through processes such as oxidation and enzymatic reactions. Tosif et al. (2023) found a similar trend for the antioxidant activity of the fresh-cut apples coated with *aloe vera* and carboxymethyl cellulose. Ultimately, the findings indicate that applying an AMFSP coating to apples could potentially prolong their antioxidant properties when compared to apples without a coating.

3.6.5. Microbial analysis

Microbial analysis of cut apple fruit samples over 10 days (Fig. 6F) revealed that initially, on the 0^{th} day, no microbial contamination was found in both samples. However, by the 10^{th} day of analysis, there was a significant increase ($p < 0.05$) in total plate count (TPC) for the control sample (0.94 ± 0.07 log CFU/g) compared to the coated sample (0.76 ± 0.10 log CFU/g). Similarly, yeast and mold counts in the control sample (0.52 ± 0.06 log CFU/g) showed a significant increase ($p < 0.05$) compared to the coated sample (0.47 ± 0.14 log CFU/g) by the 10^{th} day of analysis. The results indicate that coating the fresh-cut apple with AMFSP effectively reduces bacterial and yeast and mold growth compared to uncoated apples, likely due to the coating which acts as a physical barrier, limiting microbial access to nutrients and moisture essential for their proliferation (Ghosh & Singh, 2022). Additionally, the polysaccharides may possess inherent antimicrobial properties, further inhibiting microbial growth. The coating also regulates moisture levels on the apple surface, creating an environment less favorable for microbial growth. Overall, this study suggests that AMFSP has promising potential for extending shelf life and preserving microbial quality in food products. Similar results have been detected by (Hammad et al., 2021) for the apple coated with whey protein concentrate.

3.6.6. Sensory analysis

Sensory evaluation using the 9-point hedonic scale reveals that coating the fresh-cut apple with AMFSP affects its appearance, flavor, and texture, ultimately affecting the overall sensory attributes (Fig. 6G). At the initial stage (Day 0), the coated sample exhibits an insignificant difference ($p > 0.05$) in appearance (8) and flavor (8) as compared to the control (7.5). However, over the 10 days, there is a decline in sensory attributes for both coated and control samples. By Day 10, the coated sample maintained slightly higher scores in appearance (6) and flavor (6.5) compared to the control (5.5), indicating a potential preservation effect of the coating on sensory qualities. Both samples exhibited a

decline in texture attributes over time, with the coated sample continuously achieving somewhat higher scores than the control. The overall scores exhibit a consistent trend, with the coated sample consistently achieving a better score than the control over the storage period.

4. Conclusion

The application of polysaccharides extracted from *Aegle marmelos* fruit shells offers a great opportunity for sustainable value enhancement and waste minimization. The fruit shell is a significant source of bioactive compounds, particularly polysaccharides, highlighting the necessity of investigating unusual sources. The multifunctional properties of polysaccharides offer diverse applications, ranging from food preservation to environmental remediation. The ability of polysaccharides to act as edible coatings on fresh-cut fruits, such as apples, not only extends shelf life by providing a protective barrier against microbial contamination and moisture loss but also aligns with consumer demand for natural and eco-friendly packaging solutions. Additionally, polysaccharides exhibit promising capabilities in photocatalytic dye reduction, contributing to the mitigation of environmental pollution from synthetic dyes in industrial effluents.

CRediT authorship contribution statement

Madhu Sharma: Writing – original draft, Methodology, Investigation, Formal analysis, Data curation. **Aarti Bains:** Writing – review & editing, Methodology. **Gulden Goksen:** Methodology, Validation, Data curation, Visualization, Writing – review & editing. **Nemat Ali:** Writing – review & editing, Methodology. **Mohammad Rashid Khan:** Writing – review & editing, Methodology. **Gulsah Karabulut:** Writing – review & editing, Validation, Supervision, Resources, Funding acquisition. **Prince Chawla:** Writing – review & editing, Supervision, Project administration, Methodology, Investigation, Formal analysis, Conceptualization.

Declaration of competing interest

The authors declare that they have no known competing financial interests or personal relationships that could have appeared to influence the work reported in this paper.

Data availability

Data will be made available on request.

Acknowledgements

The support of Central Instrument Facility, Lovely Professional University is greatfully acknowledged also authors are thankful to the Researchers Supporting Project Number (RSPD2024R940), King Saud University, Riyadh, Saudi Arabia, and Sakarya University, Türkiye for supporting this study.

References

Aayush, K., McClements, D. J., Sharma, S., Sharma, R., Singh, G. P., Sharma, K., & Oberoi, K. (2022). Innovations in the development and application of edible coatings for fresh and minimally processed apple. *Food Control, 141*(109188), Article 109188. https://doi.org/10.1016/j.foodcont.2022.109188

Abbas, M., Ahmed, D., Qamar, M. T., Ihsan, S., & Noor, Z. I. (2021). Optimization of ultrasound-assisted, microwave-assisted and Soxhlet extraction of bioactive compounds from *Lagenaria siceraria*: A comparative analysis. *Bioresource Technology Reports, 15*(100746), Article 100746. https://doi.org/10.1016/j.biteb.2021.100746

Ahmad, S., Aadil, M., Ejaz, S. R., Akhtar, M. U., Noor, H., Haider, S., … Yasmin, G. (2022). Sol-gel synthesis of nanostructured ZnO/$SrZnO_2$ with boosted antibacterial and photocatalytic activity. *Ceramics International, 48*(2), 2394–2405. https://doi.org/10.1016/j.ceramint.2021.10.020

Ali, S., Akbar Anjum, M., Sattar Khan, A., Nawaz, A., Ejaz, S., Khaliq, G., Iqbal, S., Ullah, S., Naveed Ur Rehman, R., Moaaz Ali, M., & Shahzad Saleem, M. (2022). Carboxymethyl cellulose coating delays ripening of harvested mango fruits by regulating softening enzymes activities. *Food Chemistry, 380*(131804), Article 131804. https://doi.org/10.1016/j.foodchem.2021.131804

Arab, K., Ghanbarzadeh, B., Ayaseh, A., & Jahanbin, K. (2021). Extraction, purification, physicochemical properties and antioxidant activity of a new polysaccharide from *Ocimum album* L. seed. *International Journal of Biological Macromolecules, 180*, 643–653. https://doi.org/10.1016/j.ijbiomac.2021.03.088

Arnold, M., & Gramza-Michałowska, A. (2022). Enzymatic browning in apple products and its inhibition treatments: A comprehensive review. *Comprehensive Reviews in Food Science and Food Safety, 21*, 5038–5076.

Bazezew, A. M., Admassu Emire, S., Teamir Sisay, M., & Kinyuru, J. (2022). Extraction, phytochemical analysis, monosaccharide composition and functional properties of *X. americana* seed mucilage. *Bioactive Carbohydrates and Dietary Fibre, 27*(100302), Article 100302. https://doi.org/10.1016/j.bcdf.2021.100302

Beyaz, A., Ozturk, R., & Turker, U. (2010). Assessment of mechanical damage on apples with image analysis. *Journal: Food, Agriculture & Environment (JFAE), 8*(3 & 4), 476–480.

Biswas, S., & Rashid, T. U. (2022). Effect of ultrasound on the physical properties and processing of major biopolymers-a review. *Soft Matter, 18*(44), 8367–8383. https://doi.org/10.1039/d2sm01339h

Chavan, P., Sharma, P., Sharma, S. R., Mittal, T. C., & Jaiswal, A. K. (2022). Application of high-intensity ultrasound to improve food processing efficiency: A review. *Foods (Basel, Switzerland), 11*(1), 122. https://doi.org/10.3390/foods11010122

Chen, S.-K., Wang, X., Guo, Y.-Q., Song, X.-X., Yin, J.-Y., & Nie, S.-P. (2023). Exploring the partial degradation of polysaccharides: Structure, mechanism, bioactivities, and perspectives. *Comprehensive Reviews in Food Science and Food Safety, 22*(6), 4831–4870. https://doi.org/10.1111/1541-4337.13244

Chettri, S., Sharma, N., & Mohite, A. M. (2023). Utilization of lima bean starch as an edible coating base material for sapota fruit shelf-life enhancement. *Journal of Agriculture and Food Research, 12*(100615), Article 100615. https://doi.org/10.1016/j.jafr.2023.100615

Colusse, G. A., Carneiro, J., Duarte, M. E. R., Carvalho, J. C.d., & Noseda, M. D. (2022). Advances in microalgal cell wall polysaccharides: A review focused on structure, production, and biological application. *Critical Reviews in Biotechnology, 42*(4), 562–577. https://doi.org/10.1080/07388551.2021.1941750

Dong, R., Huang, Z., Ma, W., Yu, Q., Xie, J., Tian, J., Li, B., Shan, J., & Chen, Y. (2024). Fabrication of nanocomplexes for anthocyanins delivery by ovalbumin and differently dense sulphate half-ester polysaccharides nanocarriers: Enhanced stability, bio-accessibility, and antioxidant properties. *Food Chemistry, 432*(137263), Article 137263. https://doi.org/10.1016/j.foodchem.2023.137263

El Idrissi, A., Channab, B. E., Essamlali, Y., & Zahouily, M. (2023). Superabsorbent hydrogels based on natural polysaccharides: Classification, synthesis, physicochemical properties, and agronomic efficacy under abiotic stress conditions: A review. *International Journal of Biological, 258*, 128909.

Feng, S., Zhang, J., Luo, X., Xu, Z., Liu, K., Chen, T., Zhou, L., & Ding, C. (2023). Green extraction of polysaccharides from Camellia oleifera fruit shell using tailor-made deep eutectic solvents. *International Journal of Biological Macromolecules, 253*(Pt 6), Article 127286. https://doi.org/10.1016/j.ijbiomac.2023.127286

Gao, X., Yin, H., Li, M., Xin, L., Zhang, H., & Long, H. (2023). Photocatalytic degradation of methyl orange by a diethylenetriamine modified chitosan/bentonite composite. *Reaction Chemistry & Engineering, 8*(10), 2505–2521.

Gaikwad, D., Sutar, R., & Patil, D. (2024). Polysaccharide mediated nanodrug delivery: A review. *International Journal of Biological Macromolecules, 261*, 129547.

Gao, X., Yin, H., Guo, C., Yan, B., Li, M., Xin, L., & Wu, Z. (2023). Comprehensive removal of various dyes by thiourea modified chitosan/nano ZnS composite via enhanced photocatalysis: Performance and mechanism. *International Journal of Biological Macromolecules, 247*(125677), Article 125677. https://doi.org/10.1016/j.ijbiomac.2023.125677

Ghosh, M., & Singh, A. K. (2022). Potential of engineered nanostructured biopolymer based coatings for perishable fruits with coronavirus safety perspectives. *Progress in Organic Coatings, 163*(106632), Article 106632. https://doi.org/10.1016/j.porgcoat.2021.106632

Gouda, M., El-Din Bekhit, A., Tang, Y., Huang, Y., Huang, L., He, Y., & Li, X. (2021). Recent innovations of ultrasound green technology in herbal phytochemistry: A review. *Ultrasonics Sonochemistry, 73*(105538), Article 105538. https://doi.org/10.1016/j.ultsonch.2021.105538

Guleria, S., Simsek, H., Chawla, P., Relhan, A., & Bhasin, A. (2024). Evaluation of Cladophora and Chlamydomonas microalgae for environmental sustainability: A comparative study of antimicrobial and photocatalytic dye degradation. *Environmental Pollution (Barking, Essex: 1987), 340*(122806), Article 122806. https://doi.org/10.1016/j.envpol.2023.122806

Hammad, K. S. M., Elsayed, N., & Elkashef, H. (2021). Development of a whey protein concentrate/apple pomace extract edible coating for shelf life extension of fresh-cut apple. *International Food Research Journal, 28*(2), 377–385. https://doi.org/10.47836/ifrj.28.2.19

Hashim, S. S., Jubier, N. J., & Hasan, S. M. (2024). Structural and morphological study for polymerized polypyrrole/cu nanocomposites. In , *Vol. 2922. AIP conference proceedings*. AIP Publishing.

Hassanbeiki, M., Golestan, L., Mashak, Z., Ahmadi, M., & Jafari, S. M. (2024). Production of a functional confectionary cream containing licorice root extract and double coated *Lactobacillus plantarum* by alginate and malva mucilage. *Carbohydrate Polymer Technologies and Applications, 7*(100435), Article 100435. https://doi.org/10.1016/j.carpta.2024.100435

Hill, C., Altgen, M., & Rautkari, L. (2021). Thermal modification of wood—A review: Chemical changes and hygroscopicity. *Journal of Materials Science, 56*(11), 6581–6614. https://doi.org/10.1007/s10853-020-05722-z

Hong, T., Yin, J.-Y., Nie, S.-P., & Xie, M.-Y. (2021). Applications of infrared spectroscopy in polysaccharide structural analysis: Progress, challenge and perspective. *Food Chemistry: X, 12*(100168), Article 100168. https://doi.org/10.1016/j.fochx.2021.100168

Hu, X., Xu, F., Li, J., Li, J., Mo, C., Zhao, M., & Wang, L. (2022). Ultrasonic-assisted extraction of polysaccharides from coix seeds: Optimization, purification, and in vitro digestibility. *Food Chemistry, 374*(131636), Article 131636. https://doi.org/10.1016/j.foodchem.2021.131636

Jönsson, M., Allahgholi, L., Sardari, R. R. R., Hreggviðsson, G. O., & Nordberg Karlsson, E. (2020). Extraction and modification of macroalgal polysaccharides for current and next-generation applications. *Molecules (Basel, Switzerland), 25*(4), 930. https://doi.org/10.3390/molecules25040930

Jung, S.-K., & Choi, H.-S. (2021). Fruit quality and antioxidant activities of yellow-skinned apple cultivars coated with natural sucrose monoesters. *Sustainability, 13*(5), 2423. https://doi.org/10.3390/su13052423

Kathiresan, S., & Lasekan, O. (2019). Effects of glycerol and stearic acid on the performance of chickpea starch-based coatings applied to fresh-cut papaya. *CyTA Journal of Food, 17*(1), 365–374. https://doi.org/10.1080/19476337.2019.1585959

Khadhraoui, B., Ummat, V., Tiwari, B. K., Fabiano-Tixier, A. S., & Chemat, F. (2021). Review of ultrasound combinations with hybrid and innovative techniques for extraction and processing of food and natural products. *Ultrasonics Sonochemistry, 76*(105625), Article 105625. https://doi.org/10.1016/j.ultsonch.2021.105625

Kocira, A., Kozłowicz, K., Panasiewicz, K., Staniak, M., Szpunar-Krok, E., & Hortyńska, P. (2021). Polysaccharides as edible films and coatings: Characteristics and influence on fruit and vegetable quality—A review. *Agronomy (Basel, Switzerland), 11*(5), 813. https://doi.org/10.3390/agronomy11050813

Kumar, A., Sharma, G., Naushad, M., Al-Muhtaseb, A. H., García-Peñas, A., Mola, G. T., … Stadler, F. J. (2020). Bio-inspired and biomaterials-based hybrid photocatalysts for environmental detoxification: A review. *Chemical Engineering Journal (Lausanne, Switzerland: 1996), 382*(122937), Article 122937. https://doi.org/10.1016/j.cej.2019.122937

Li, X., Zhang, L., Yang, Z., Wang, P., Yan, Y., & Ran, J. (2020). Adsorption materials for volatile organic compounds (VOCs) and the key factors for VOCs adsorption process: A review. *Separation and Purification Technology, 235*(116213), Article 116213. https://doi.org/10.1016/j.seppur.2019.116213

Liu, X., Xu, S., Ding, X., Yue, D., Bian, J., Zhang, X., … Gao, P. (2020). Structural characteristics of *Medicago Sativa* L. polysaccharides and Se-modified polysaccharides as well as their antioxidant and neuroprotective activities. *International Journal of Biological Macromolecules, 147*, 1099–1106. https://doi.org/10.1016/j.ijbiomac.2019.10.078

Liu, Y., Zhao, Y., & Wang, J. (2021). Fenton/Fenton-like processes with in-situ production of hydrogen peroxide/hydroxyl radical for degradation of emerging contaminants: Advances and prospects. *Journal of Hazardous Materials, 404*(Pt B), Article 124191. https://doi.org/10.1016/j.jhazmat.2020.124191

Mahato, H., & Kumar, B. (2022). *Medicinal uses with immense economic potential and nutritional properties of Aegle marmelos: A concise review. Biocomposites.* Norderstedt.133: Books on Demand.

Maringgal, B., Hashim, N., Mohamed Amin Tawakkal, I. S., & Muda Mohamed, M. T. (2020). Recent advance in edible coating and its effect on fresh/fresh-cut fruits quality. *Trends in Food Science & Technology, 96*, 253–267. https://doi.org/10.1016/j.tifs.2019.12.024

Medlej, M. K., Cherri, B., Nasser, G., Zaviska, F., Hijazi, A., Li, S., & Pochat-Bohatier, C. (2020). Optimization of polysaccharides extraction from a wild species of Ornithogalum combining ultrasound and maceration and their anti-oxidant properties. *International Journal of Biological Macromolecules, 161*, 958–968. https://doi.org/10.1016/j.ijbiomac.2020.06.021

Mohammad, A. A., Mehaya, F. M., Salem, S. H., & Amer, H. M. (2024). Psyllium and okra mucilage as co-carrier wall materials for fenugreek oil encapsulation and its utilization as fat replacers in pan bread and biscuit production. *Heliyon, 10*(3), Article e25321. https://doi.org/10.1016/j.heliyon.2024.e25321

Mohammed, J. K., Mahdi, A. A., Ahmed, M. I., Ma, M., & Wang, H. (2020). Preparation, deproteinization, characterization, and antioxidant activity of polysaccharide from Medemia argun fruit. *International Journal of Biological Macromolecules, 155*, 919–926. https://doi.org/10.1016/j.ijbiomac.2019.11.050

Mtibe, A., Motloung, M. P., Bandyopadhyay, J., & Ray, S. S. (2021). Synthetic biopolymers and their composites: Advantages and limitations-an overview. *Macromolecular Rapid Communications, 42*(15), Article e2100130. https://doi.org/10.1002/marc.202100130

Muhammad, A., Shah, A.u. H. A., & Bilal, S. (2020). Effective adsorption of hexavalent chromium and divalent nickel ions from water through polyaniline, iron oxide, and their composites. *Applied Sciences (Basel, Switzerland), 10*(8), 2882. https://doi.org/10.3390/app10082882

Nadendla, R. R., Rao, K. S., Kanna, S., Satyanarayana, J., & Mrudhvani, C. (2024). Preparation and evaluation of spray dried powder of Trigonella foenum-graecum seeds as suspending agents to develop rivaroxaban nanosuspension. *Indian Journal of Biochemistry and Biophysics (IJBB), 61*(2), 105–117.

Ognyanov, M., Remoroza, C., Schols, H. A., Georgiev, Y. N., Petkova, N. T., & Krystyjan, M. (2020). Structural, rheological and functional properties of galactose-rich pectic polysaccharide fraction from leek. *Carbohydrate Polymers, 229*(115549), Article 115549. https://doi.org/10.1016/j.carbpol.2019.115549

Olawuyi, I. F., Kim, S. R., Hahn, D., & Lee, W. Y. (2020). Influences of combined enzyme-ultrasonic extraction on the physicochemical characteristics and properties of okra polysaccharides. *Food Hydrocolloids, 100*(105396), Article 105396. https://doi.org/10.1016/j.foodhyd.2019.105396

Oliveira Filho, J. G.d., Silva, G.d. C., Oldoni, F. C. A., Miranda, M., Florencio, C., Oliveira, R. M. D.d., … Ferreira, M. D. (2022). Edible coating based on carnauba wax nanoemulsion and Cymbopogon martinii essential oil on papaya postharvest preservation. *Coatings, 12*(11), 1700. https://doi.org/10.3390/coatings12111700

Onwude, D. I., Chen, G., Eke-emezie, N., Kabutey, A., Khaled, A. Y., & Sturm, B. (2020). Recent advances in reducing food losses in the supply chain of fresh agricultural produce. *Processes (Basel, Switzerland), 8*(11), 1431. https://doi.org/10.3390/pr8111431

Pandey, S., Do, J. Y., Kim, J., & Kang, M. (2020). Fast and highly efficient catalytic degradation of dyes using κ-carrageenan stabilized silver nanoparticles nanocatalyst. *Carbohydrate Polymers, 230*(115597), Article 115597. https://doi.org/10.1016/j.carbpol.2019.115597

Pochapski, Daniel José, Carvalho Dos Santos, C., Leite, G. W., Pulcinelli, S. H., & Santilli, C. V. (2021). Zeta potential and colloidal stability predictions for inorganic nanoparticle dispersions: Effects of experimental conditions and electrokinetic models on the interpretation of results. *Langmuir, 37*(45), 13379–13389. https://doi.org/10.1021/acs.langmuir.1c02056

Purwandari, F. A., Westerbos, C., Lee, K., Fogliano, V., & Capuano, E. (2023). Proximate composition, microstructure, and protein and starch digestibility of seven collections of Jack bean (Canavalia ensiformis) with different optimal cooking times. *Food Research International, 170*, 112956.

Riaz, A., Aadil, R. M., Amoussa, A. M. O., Bashari, M., Abid, M., & Hashim, M. M. (2021). Application of chitosan-based apple peel polyphenols edible coating on the preservation of strawberry (Fragaria ananassa cv Hongyan) fruit. *Journal of Food Processing and Preservation, 45*(1).

Sarkar, S., Ponce, N. T., Banerjee, A., Bandopadhyay, R., Rajendran, S., & Lichtfouse, E. (2020). Green polymeric nanomaterials for the photocatalytic degradation of dyes: A review. *Environmental Chemistry Letters, 18*(5), 1569–1580. https://doi.org/10.1007/s10311-020-01021-w

Savi, A., Calegari, G. C., Santos, V. A. Q., Pereira, E. A., & Teixeira, S. D. (2020). Chemical characterization and antioxidant of polysaccharide extracted from *Dioscorea bulbifera*. *Journal of King Saud University, Science, 32*(1), 636–642. https://doi.org/10.1016/j.jksus.2018.09.002

Sharma, M., Bains, A., Sridhar, K., Chawla, P., & Sharma, M. (2023). Process optimization for spray dried *Aegle marmelos* fruit nanomucilage: Characterization, functional properties, and in vitro antibiofilm activity against food pathogenic microorganisms. *International Journal of Biological Macromolecules, 249*, Article 126050. https://doi.org/10.1016/j.ijbiomac.2023.126050

Sharma, N., Radha, Kumar, M., Zhang, B., Kumari, N., Singh, D., … Lorenzo, J. M. (2022). *Aegle marmelos* (L.) Correa: An underutilized fruit with high nutraceutical values: A review. *International Journal of Molecular Sciences, 23*(18). https://doi.org/10.3390/ijms231810889

Shen, S., Zhou, C., Zeng, Y., Zhang, H., Hossen, M. A., Dai, J., … Liu, Y. (2022). Structures, physicochemical and bioactive properties of polysaccharides extracted from Panax notoginseng using ultrasonic/microwave-assisted extraction. *Lebensmittel-Wissenschaft Und Technologie [Food Science and Technology], 154*(112446), Article 112446. https://doi.org/10.1016/j.lwt.2021.112446

Shrestha, L., Kulig, B., Moscetti, R., Massantini, R., Pawelzik, E., Hensel, O., & Sturm, B. (2020). Optimisation of physical and chemical treatments to control browning development and enzymatic activity on fresh-cut apple slices. *Foods (Basel, Switzerland), 9*(1), 76. https://doi.org/10.3390/foods9010076

Slama, H. B., Chenari Bouket, A., Pourhassan, Z., Alenezi, F. N., Silini, A., Cherif-Silini, H., … Belbahri, L. (2021). Diversity of synthetic dyes from textile industries, discharge impacts and treatment methods. *Applied Sciences (Basel, Switzerland), 11*(14), 6255. https://doi.org/10.3390/app11146255

Soeung, R., Felipe, L.d. O., Bouhoute, M., Taarji, N., Nakajima, M., & Neves, M. A. (2022). Limnophila aromatica crude extracts as natural emulsifiers for formation and stabilizing of oil-in-water (O/W) emulsions. *Colloids and Interfaces, 6*(2), 26. https://doi.org/10.3390/colloids6020026

Solís-Contreras, G. A., Rodríguez-Guillermo, M. C., de la Luz Reyes-Vega, M., Aguilar, C. N., Rebolloso-Padilla, O. N., Corona-Flores, J., … Ruelas-Chacon, X. (2021). Extending shelf-life and quality of minimally processed Golden delicious apples with three bioactive coatings combined with cinnamon essential oil. *Foods (Basel, Switzerland), 10*(3), 597. https://doi.org/10.3390/foods10030597

Su, Y., & Li, L. (2020). Structural characterization and antioxidant activity of polysaccharide from four auriculariales. *Carbohydrate Polymers, 229*(115407), Article 115407. https://doi.org/10.1016/j.carbpol.2019.115407

Sun, H., Jiao, R., An, G., Xu, H., & Wang, D. (2021). Influence of particle size on the aggregation behavior of nanoparticles: Role of structural hydration layer. *Journal of Environmental Sciences (China), 103*, 33–42. https://doi.org/10.1016/j.jes.2020.10.007

Surolia, R., Singh, A., & Bhatnagar, T. (2022). Comparative study on the characterization and antioxidant properties of Bael (*Aegle Marmelos*) pulp, Shell and Seed Pectin. In *Research Square*. https://doi.org/10.21203/rs.3.rs-1586407/v1

Surya, S., Sindhusha, S., & Gunasekaran, B. (2023). Synthesis, structural, optical, thermal, electrical, nonlinear optical and theoretical investigation on 3-aminopyridine picrate (3APP) single crystal. *Journal of Molecular Structure, 1272*(134259), Article 134259. https://doi.org/10.1016/j.molstruc.2022.134259

Tabassum, N., & Khan, M. A. (2020). Modified atmosphere packaging of fresh-cut papaya using alginate based edible coating: Quality evaluation and shelf life study. *Scientia Horticulturae, 259*(108853), Article 108853. https://doi.org/10.1016/j.scienta.2019.108853

Tamo, A. K. (2024). Nanocellulose-based hydrogels as versatile bio-based materials with interesting functional properties for tissue engineering applications. *Journal of Materials Chemistry, 12*, 7692–7759.

Tosif, M. M., Bains, A., Dhull, S. B., Chawla, P., & Goksen, G. (2023). Effect of *Aloe vera* and carboxymethyl cellulose-derived binary blend edible coating on the shelf life of

fresh-cut apple. *Food Science & Nutrition, 11*(11), 6987–6999. https://doi.org/10.1002/fsn3.3623

Trenkenschuh, E., & Friess, W. (2021). Freeze-drying of nanoparticles: How to overcome colloidal instability by formulation and process optimization. *European Journal of Pharmaceutics and Biopharmaceutics: Official Journal of Arbeitsgemeinschaft Für Pharmazeutische Verfahrenstechnik e.V, 165*, 345–360. https://doi.org/10.1016/j.ejpb.2021.05.024

Wang, C., Li, J., Cao, Y., Huang, J., Lin, H., Zhao, T., Liu, L., Shen, P., Julian McClements, D., Chen, J., Liu, C., Liu, J., & Li, Q. (2023). Extraction and characterization of pectic polysaccharides from *Choerospondias axillaris* peels: Comparison of hot water and ultrasound-assisted extraction methods. *Food Chemistry, 401*(134156), Article 134156. https://doi.org/10.1016/j.foodchem.2022.134156

Wang, D., Ma, Q., Li, D., Li, W., Li, L., Aalim, H., & Luo, Z. (2021). Moderation of respiratory cascades and energy metabolism of fresh-cut pear fruit in response to high CO2 controlled atmosphere. *Postharvest Biology and Technology, 172*(111379), Article 111379. https://doi.org/10.1016/j.postharvbio.2020.111379

Wang, S., Yang, J., Shao, G., Qu, D., Zhao, H., Yang, L., … Zhu, D. (2020). Soy protein isolated-soy hull polysaccharides stabilized O/W emulsion: Effect of polysaccharides concentration on the storage stability and interfacial rheological properties. *Food Hydrocolloids, 101*(105490), Article 105490. https://doi.org/10.1016/j.foodhyd.2019.105490

Wang, S., Li, G., Zhang, X., Wang, Y., Qiang, Y., Wang, B., … Wang, Z. (2022). Structural characterization and antioxidant activity of Polygonatum sibiricum polysaccharides. *Carbohydrate Polymers, 291*(119524), Article 119524. https://doi.org/10.1016/j.carbpol.2022.119524

Wu, J., Chen, R., Tan, L., Bai, H., Tian, L., Lu, J., Gao, M., Bai, C., Sun, H., & Chi, Y. (2022). Ultrasonic disruption effects on the extraction efficiency, characterization, and bioactivities of polysaccharides from Panax notoginseng flower. *Carbohydrate Polymers, 291*(119535), Article 119535. https://doi.org/10.1016/j.carbpol.2022.119535

Yan, B., Dai, Y., Xin, L., Li, M., Zhang, H., Long, H., & Gao, X. (2024). Research progress in the degradation of printing and dyeing wastewater using chitosan based composite photocatalytic materials. *International Journal of Biological Macromolecules, 263*(Pt 2), Article 130082. https://doi.org/10.1016/j.ijbiomac.2024.130082

Yang, X., Li, A., Li, X., Sun, L., & Guo, Y. (2020). An overview of classifications, properties of food polysaccharides and their links to applications in improving food textures. *Trends in Food Science & Technology, 102*, 1–15. https://doi.org/10.1016/j.tifs.2020.05.020

Yang, Y., Qiu, Z., Li, L., Vidyarthi, S. K., Zheng, Z., & Zhang, R. (2021). tructural characterization and antioxidant activities of one neutral polysaccharide and three acid polysaccharides from *Ziziphus jujuba* cv. Hamidazao: A comparison. *Carbohydrate, 261*, 117879.

Yu, J., Wang, X.-Y., Li, D., Wang, L.-J., & Wang, Y. (2022). Development of soy protein isolate emulsion gels as extrusion-based 3D food printing inks: Effect of polysaccharides incorporation. *Food Hydrocolloids, 131*(107824), Article 107824. https://doi.org/10.1016/j.foodhyd.2022.107824

Zhai, X., Lin, D., Li, W., & Yang, X. (2020). Improved characterization of nanofibers from bacterial cellulose and its potential application in fresh-cut apples. *International Journal of Biological Macromolecules, 149*, 178–186. https://doi.org/10.1016/j.ijbiomac.2020.01.230

Zhou, S., Rahman, A., Li, J., Wei, C., Chen, J., Linhardt, R. J., … Chen, S. (2020). Extraction methods affect the structure of Goji (*Lycium barbarum*) polysaccharides. *Molecules (Basel, Switzerland), 25*(4). https://doi.org/10.3390/molecules25040936

Zhou, S., & Huang, G. (2023). Extraction, purification and antioxidant activity of Juglans regia shell polysaccharide. *Chemical and Biological Technologies in Agriculture, 10*(1). https://doi.org/10.1186/s40538-023-00447-y

Song, K., Liu, Y., Umar, A., Ma, H., & Wang, H. (2023). Ultrasonic cavitation: Tackling organic pollutants in wastewater. *Chemosphere, 350*, 141024.